Evaluation of Cross Section Data for the Low and Medium Energy Cyclotron Production of the Non-Standard Positron Emitting Radionuclide ^{90}Nb

Ahmad Naz[a], N. Amjed[a,1], A. M. Wajid[a], M. Hussain[b, c], S.M. Qaim[b]

[a] Department of Physics, Division of Science and Technology, University of Education, Lahore, Pakistan

[b] Institut für Neurowissenschaften und Medizin, INM-5: Nuklearchemie, Forschungszentrum Jülich GmbH, D-52425 Jülich, Germany.

[c] Department of Physics, Government College University Lahore, Lahore 54000, Pakistan

Abstract: The radionuclide ^{90}Nb ($T_{1/2}$ = 14.60) is a promising non-standard β^+-emitter, with potential to be used in Immuno-PET. Its production was studied using ^{90}Zr, ^{91}Zr, ^{93}Nb and ^{89}Y targets. Experimental excitation functions of the reactions ^{90}Zr(p,n)^{90}Nb, ^{91}Zr(p,2n)^{90}Nb, ^{90}Zr(d,2n)^{90}Nb, ^{93}Nb(p,4n)^{90}Mo(→^{90}Nb) and ^{89}Y(α,3n)^{90}Nb were critically analyzed. The nuclear model codes TALYS 1.9, ALICE-IPPE, and EMPIRE 3.2 were employed to check the consistency and reliability of the experimental data. A well-developed methodology, based on the experimental data and the results of theoretical nuclear models, was used to calculate the recommended data for each excitation function. The same was done for reactions leading to possible radioisotopic impurities. By using the recommended/reference data, thick target yields were calculated for each production route and its corresponding impurity reactions. After a careful analysis and comparison of all production routes, it is concluded that the ^{90}Zr(p,n)^{90}Nb reaction is better for low energy cyclotrons, and the ^{91}Zr(p,2n)^{90}Nb and^{90}Zr(d,2n)^{90}Nb reactions are suitable for medium energy cyclotrons. The routes namely ^{93}Nb(p,4n)^{90}Mo→^{90}Nb and ^{89}Y(α,3n)^{90}Nb are suitable for high energy cyclotrons. For each of these production routes, an optimum energy range is suggested. The recommended results for ^{90}Zr(p,n)^{90}Nb and ^{91}Zr(p,2n)^{90}Nb reactions were validated by comparison with the data for the ^{nat}Zr(p,x)^{90}Nb process.

Keywords:

Cyclotron production

Niobium 90

Immuno PET

[1] Corresponding author.
E-mail address: noumanamjad@ue.edu.pk (N. Amjed)
noumanamjad@yahoo.co
Phone No: +923216026570

Proton, deuteron, and alpha particle induced reactions

Nuclear model calculation

Evaluated nuclear data

Thick target yield

Highlights;

- Evaluation of excitation functions of ^{90}Zr(p,n)^{90}Nb, ^{93}Nb(p,4n)^{90}Mo and ^{89}Y(α,3n)^{90}Nb reactions.
- Suggested cross sections for ^{90}Zr (d,2n)^{90}Nb and ^{91}Zr(p,2n)^{90}Nb reactions
- Detailed nuclear model calculations (TALYS 1.9, ALICE-IPPE, and EMPIRE 3.2) and statistical fitting of the selected data.
- Estimation of integral yield and impurity level in the production of ^{90}Nb.
- Validation of recommended cross sections by comparison with ^{nat}Zr(p,x)^{90}Nb reaction

1 Introduction

^{90}Nb is one of the promising radionuclides to be used in Immuno-PET. Immuno-PET is a rapidly growing branch of Positron Emission Tomography (PET) imaging that is mainly based on the use of biomolecules like antibody fragments labeled with the positron emitting radionuclides to obtain selective tumor imaging (Wu, 2009; van Dongen and Vosjan, 2010; Marik and Junutula, 2011). This requires a radionuclide with a half-life which correlates well with the biological kinetics of the biomolecule under investigation and which can be attached to the proteins by robust labeling chemistry (Radchenko et al., 2014; Radchenko et al., 2016). The choice of the radionuclide for application in Immuno-PET is important to determine overall properties as well as in the formation of radioimmunoconjugate (Boswell and Brechbiel, 2007).

^{90}Nb ($T_{1/2}$=14.6 h) is a potential candidate for PET because it has an intermediate half-life that is appropriate for studying monoclonal antibodies and antibody fragments. ^{90}Nb-labeled antibody rituximab is highly stable and the mean β^+ energy of 660 keV with 53% intensity offers high resolution in PET (Radchenko et al., 2016), which allows the visualization and quantification of biological processes with medium and slow kinetics (Radchenko et al., 2014).

^{90}Nb has a very short lived ($T_{1/2}$=18.8 s) isomeric state which decays 100% to the ground state ($T_{1/2}$=14.6 h). The decay characteristics of ^{90}Nb and of some other radionuclides encountered as impurities during its production are given in Table 1 (mainly taken from (NuDat 3.0)).

1.1 Cyclotron Production of the Radionuclide ^{90}Nb

In recent years the production of medical radioisotopes using low energy cyclotrons has been increasing significantly (Qaim, 2004.). Keeping in view the widely spreading application of PET in patient care, on-site cyclotrons are considered essential (Qaim, 2003,; Qaim, 2004.; Qaim, 2012). Cyclotron production of research oriented non-standard positron emitters is also increasing (Qaim, 2011; Qaim, 2017). Among them the radionuclide ^{90}Nb has been experimentally studied in several laboratories using the production routes ^{90}Zr(p,n)^{90}Nb, ^{91}Zr(p,2n)^{90}Nb, ^{90}Zr(d,2n)^{90}Nb, ^{89}Y(α,3n)^{90}Nb, and ^{93}Nb(p,4n)^{90}Mo→^{90}Nb.

On the IAEA database of charged particle reference cross sections, for positron emitters (Tárkányi et al., 2019) two production routes, namely ^{93}Nb(p,x)^{90}Nb and ^{89}Y(α,3n)^{90}Nb, are given for the production of ^{90}Nb. The reaction ^{93}Nb(p,x)^{90}Nb needs beam energy greater than 40 MeV and gives a good yield but with a high level of radioisotopic impurities. Furthermore, ^{90}Nb will contain significant amount of inactive Nb. If a carrier- containing radionuclide is used for immuno PET studies. It may have an adverse toxic effect on the patient (Das and Pillai, 2013). The reaction ^{89}Y(α,3n)^{90}Nb gives low yield values and this reaction also needs beam energy higher than 30 MeV (Qaim and Spahn, 2018). Proton and deuteron-induced reactions, namely ^{90}Zr(p,n)^{90}Nb, ^{91}Zr(p,2n)^{90}Nb and ^{90}Zr(d,2n)^{90}Nb, are of significant importance for high purity production of ^{90}Nb using the low and medium energy cyclotrons. For high energy region, an indirect production route namely ^{93}Nb(p,4n)^{90}Mo→^{90}Nb may be an effective method for the cyclotron production of ^{90}Nb. In general most of the investigations are limited to nuclear reaction cross section measurements. Only in the case of ^{90}Zr(p,n)^{90}Nb medium current irradiation and chemical separation have also been performed (Busse et al., 2002; Radchenko et al., 2014; Radchenko et al., 2016). The nuclear process ^{93}Nb(p,4n)^{90}Mo→^{90}Nb has been quantitatively investigated (Butement and Qaim, 1964).

The specific aim of the present work is to evaluate all possible production routes of the radionuclide ^{90}Nb, namely ^{90}Zr(p,n)^{90}Nb, ^{91}Zr(p,2n)^{90}Nb, ^{90}Zr(d,2n)^{90}Nb, ^{90}Y(α,3n)^{90}Nb and ^{93}Nb(p,4n)^{90}Mo→^{90}Nb reactions. After a careful analysis of yields and corresponding radionuclidic impurities, we suggest the suitable routes for low, medium and high energy

cyclotron production of ^{90}Nb. The literature experiments for these nuclear reactions, their Q-values, thresholds, and references are given in Table 2.

Table:2 Investigated nuclear reactions for the production of ^{90}Nb, ^{89m}Nb, and ^{91m}Nb with their Q values, threshold energies, and references

Nuclear reaction	Q-Value (MeV)	Threshold energy (MeV)	References
^{90}Zr(p,n)^{90}Nb	-6.8	6.9	(Delaunay-Olkowsky et al., 1963; Skakun et al., 1987; Levkovskij, 1991; Busse et al., 2002)
^{90}Zr(p,2n)^{89}Nb	-17.0	17.1	(Biryukov et al., 1980; Busse et al., 2002)
^{91}Zr(p,n)^{91m}Nb	-2.0	2.1	(Blaser et al., 1951; Biryukov et al., 1980)
^{91}Zr(p,2n)^{90}Nb	-14.1	14.2	(Levkovskij, 1991)
^{90}Zr(d,2n)^{90}Nb	-16.3	16.6	(Mercader et al., 1972)
^{90}Zr(d,3n)^{89}Nb	-26.4	27.0	(Usher et al., 1976)
^{89}Y(α,2n)^{91m}Nb	-14.7	15.8	(Shahid et al., 2015; Murata et al., 2019)
^{89}Y(α,3n)^{90}Nb	-26.8	28.04	(Levkovskij, 1991; Mukherjee et al., 1997; Chaubey and Rizvi, 1999; Singh et al., 2000; Shahid et al., 2015; Murata et al., 2019)
^{89}Y(α,4n)^{89}Nb	-36.9	38.6	(Chaubey and Rizvi, 1999; Murata et al., 2019)
^{93}Nb(p,4n)^{90}Mo→^{90}Nb	-32.037	32.384	(Ditrói et al., 2008; Ditroi et al., 2009; Titarenko et al., 2011; Kim et al., 2018; Voyles et al., 2018; Fox et al., 2021)

2. Evaluation Methodology

A comprehensive and well-developed evaluation methodology was used (Sudár et al., 2002; Aslam et al., 2010; Amjed et al., 2021; Amjed et al., 2022; Hussain et al., 2022). All literature experimental data were compiled using EXFOR (EXFOR) and original publications. They were then normalized based on modern standards of decay data and monitor reactions (NuDat 3.0; Tárkányi et al., 2001). Thereafter, the results of three theoretical model codes i.e., TALYS

1.9, ALICE-IPPE, and EMPIRE 3.2 were computed and compared with the experimental data. Inconsistent experimental data was deselected. Among these nuclear model codes; ALICE-IPPE is not flexible enough in adjustment of model and parameters, whereas in EMPIRE and TALYS we can adjust different models and their parameters; to get the agreement of theoretical data with experimental measurements (RIPL-3; Perey and Perey, 1963; Bojowald et al., 1988; Dityuk et al., 1998; Koning and Delaroche, 2003; Morillon and Romain, 2007; Koning and Rochman, 2012). For all three nuclear model calculations, a polynomial fit, based on the ratio of selected experimental data to model calculation, was used to normalize the excitation function of the respective theoretical model calculation. The final recommended fit was based on the average of the normalized excitation functions of all three nuclear models. This recommended fit was used to calculate the thick target yield for each reaction channel. On the basis of integral yield and contribution from radionuclidic impurities, the best production route was suggested. A suitable energy region is also suggested for the optimum production of the ^{90}Nb radionuclide.

3. Evaluation of Production Routes and Contributing Impurity Reactions

3.1 Evaluation of production data of ^{90}Nb using ^{90}Zr and ^{91}Zr targets:

3.1.1 ^{90}Zr(p,n)^{90}Nb

In literature, ^{90}Zr(p,n)^{90}Nb reaction is the most significant production route for ^{90}Nb production. The database of this reaction is fair, a total of four groups of authors, namely Busse et al. (2002), Levkovskij (1991), Skakun et al. (1987), and Delaunay-Olkowsky et al. (1963) reported experimental values of the cross section for this reaction have been given. Whereas the data by the data by Levkovskij (1991) and Busse et al. (2002) are extensive, those by Shkakun et al. (1987) and Delaunay-Olkowsky et al. (1963) only a few points in the low-energy region. The data of Levkovskij was normalized by 25% due to the difference in the cross sections of the monitor reaction (Qaim et al., 2014).

The normalized data by Levkovskij (1991) are consistent with the other three experiments. All the available normalized experimental cross sections along with the calculated results of the three nuclear model codes are shown in Figure 1. The results by TALYS 1.9 show good agreement with the experimental values while ALICE-IPPE and EMPIRE 3.2 overestimate after above 16 MeV. The overall trend of excitation functions of both experimental and theoretical values is quite similar, though with some energy shift in case of ALICE-IPPE and EMPIRE.

In the next step, according to the above-said evaluation methodology the ratio of experimental data to theoretical data by TALYS was obtained and plotted as a function of proton energy. Then the polynomial fit was obtained that was then normalized by multiplying it with the values obtained using the TALYS-1.9 nuclear model code. The same steps were repeated to normalize the values obtained using EMPIRE-3.2 and ALICE-IPPE nuclear model codes. Finally, the recommended cross sections were generated by averaging all the normalized values.

^{89}Nb as impurity

With this reaction is associated as a radioisotopic impurity produced via the ^{90}Zr(p,2n)^{89}Nb reaction. For this reaction, two experiments were found in the literature. Only one data point at 22 MeV was reported by Biryukov et al. (1980); which is rather high. The experimental data reported by Busse et al. (2002) are consistent with theoretical results, but the available information is not sufficient for evaluation. Therefore, the polynomial fit of the average of three nuclear model calculations was taken as the reference values. Recommended fit for the contributing impurity is being termed as reference value since the experimental data are scanty and a proper evaluation cannot be performed.

Selected experimental data points and fitted curves along with the 95% confidence limits for both ^{90}Nb and ^{89}Nb are shown in Figure 3 whereas numerical values are given in Table 3.

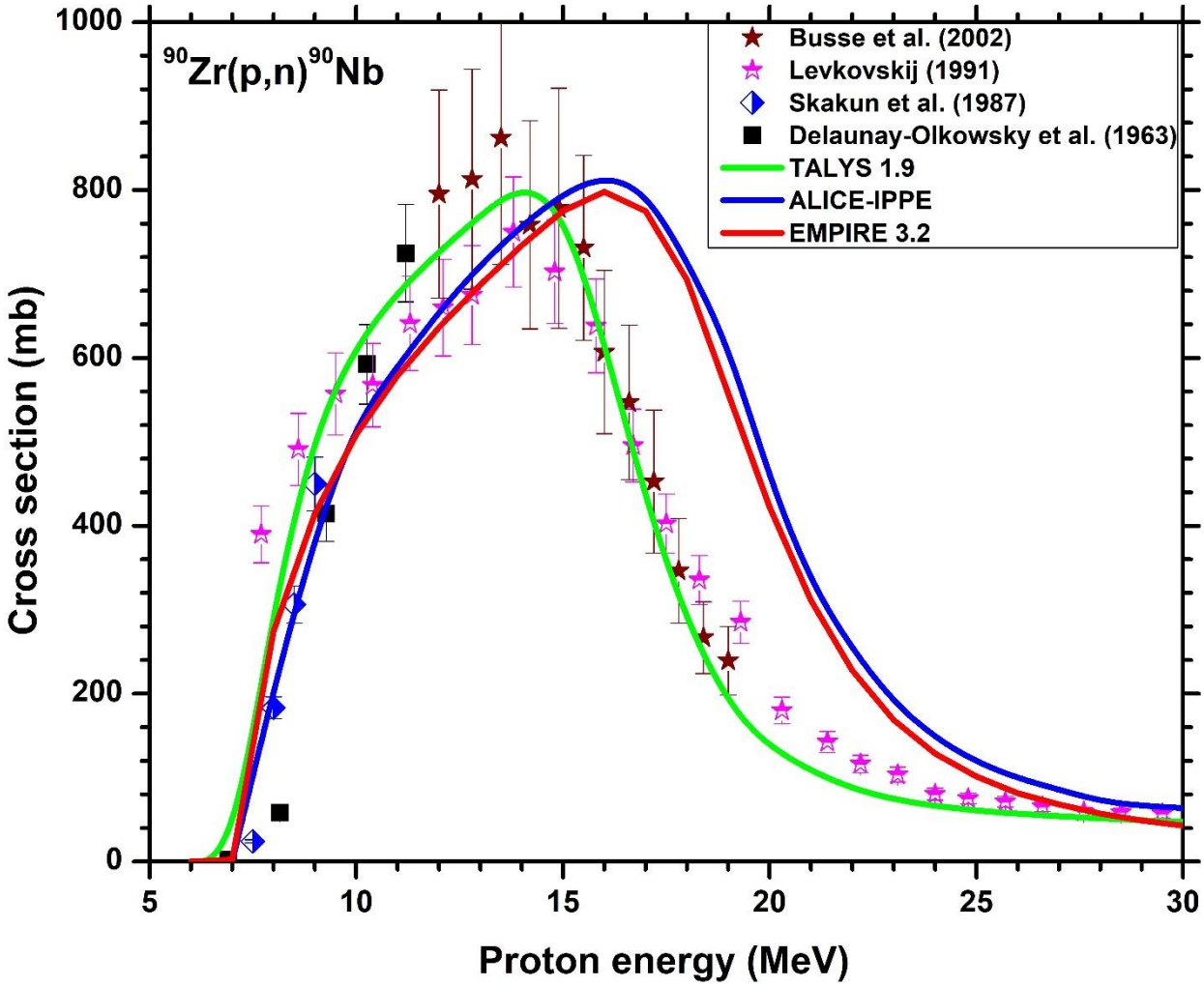

Figure 1 Normalized experimental data and results of nuclear model calculations for the ^{90}Zr(p,n)^{90}Nb reaction

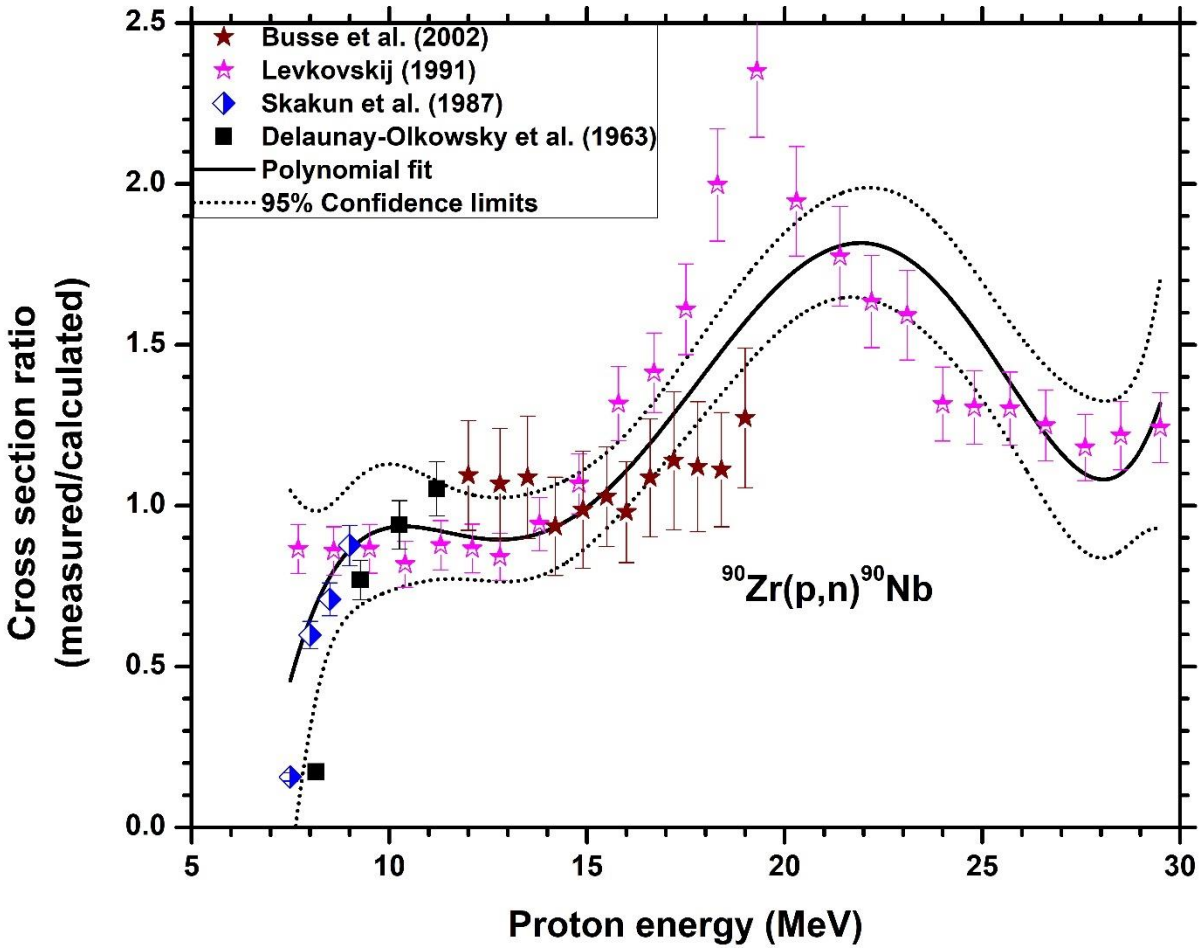

Figure 2 Ratio of measured cross section to model calculation by TALYS, plotted as a function of proton energy.

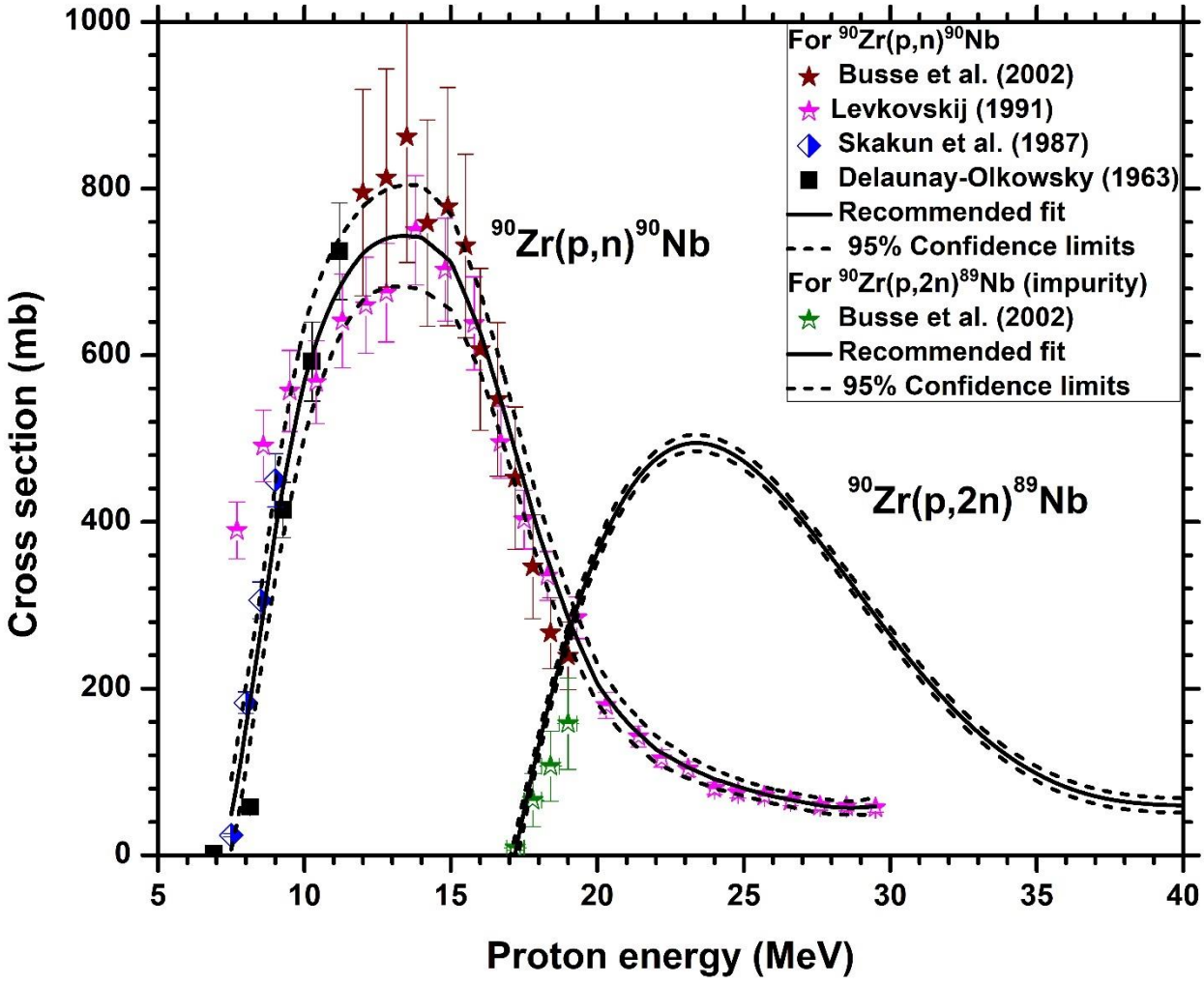

Figure 3 Selected experimental data and recommended Cross section curve with 95% upper and lower confidence limits for the ^{90}Zr(p,n)^{90}Nb and ^{90}Zr(p,2n)^{89}Nb reactions. Due to insufficient available experimental information, the latter curve should be regarded as reference curve.

3.1.2 ^{91}Zr(p,2n)^{90}Nb

^{91}Zr(p,2n)^{90}Nb also has the potential to be an effective production route for ^{90}Nb. However, the scantiness of experimental data is its limitation. In literature, only Levkovskij (1991) reported the measured values for this reaction. The data was normalized by a factor of 25 (Qaim et al., 2014).

The results of the nuclear model code TALYS 1.9 are in better agreement with the reported experimental data up to 23 MeV; afterwards, it slightly underestimates the experimental data. The overall trend of ALICE-IPPE and EMPIRE 3.2 is similar but widths of the curves are

different. Both, ALICE-IPPE and EMPIRE 3.2, underestimate the experimental values up to 21 MeV, and thereafter they slightly overestimate the experimental data (shown in Figure 4). On the whole, the results of all the model calculations describe the shape of the excitation function well.

^{89}Nb and ^{91m}Nb are two associated impurities. For the contributing impurity reactions, ^{91}Zr(p,n)^{91m}Nb and ^{91}Zr(p,3n)^{89}Nb no author has reported experimental values; therefore we relied on theoretical results. We averaged the values of nuclear model calculations. For ^{91m}Nb, the code ALICE-IPPE could not be applied, and the average was based on only two calculations. A polynomial fit of those average values was then used to generate the reference values.

Reference values for the reactions namely, ^{91}Zr(p,n)^{91m}Nb, ^{91}Zr(p,2n)^{90}Nb and ^{91}Zr(p,3n)^{89}Nb reactions are shown in Figure 5 whereas numerical values are given in Table 4.

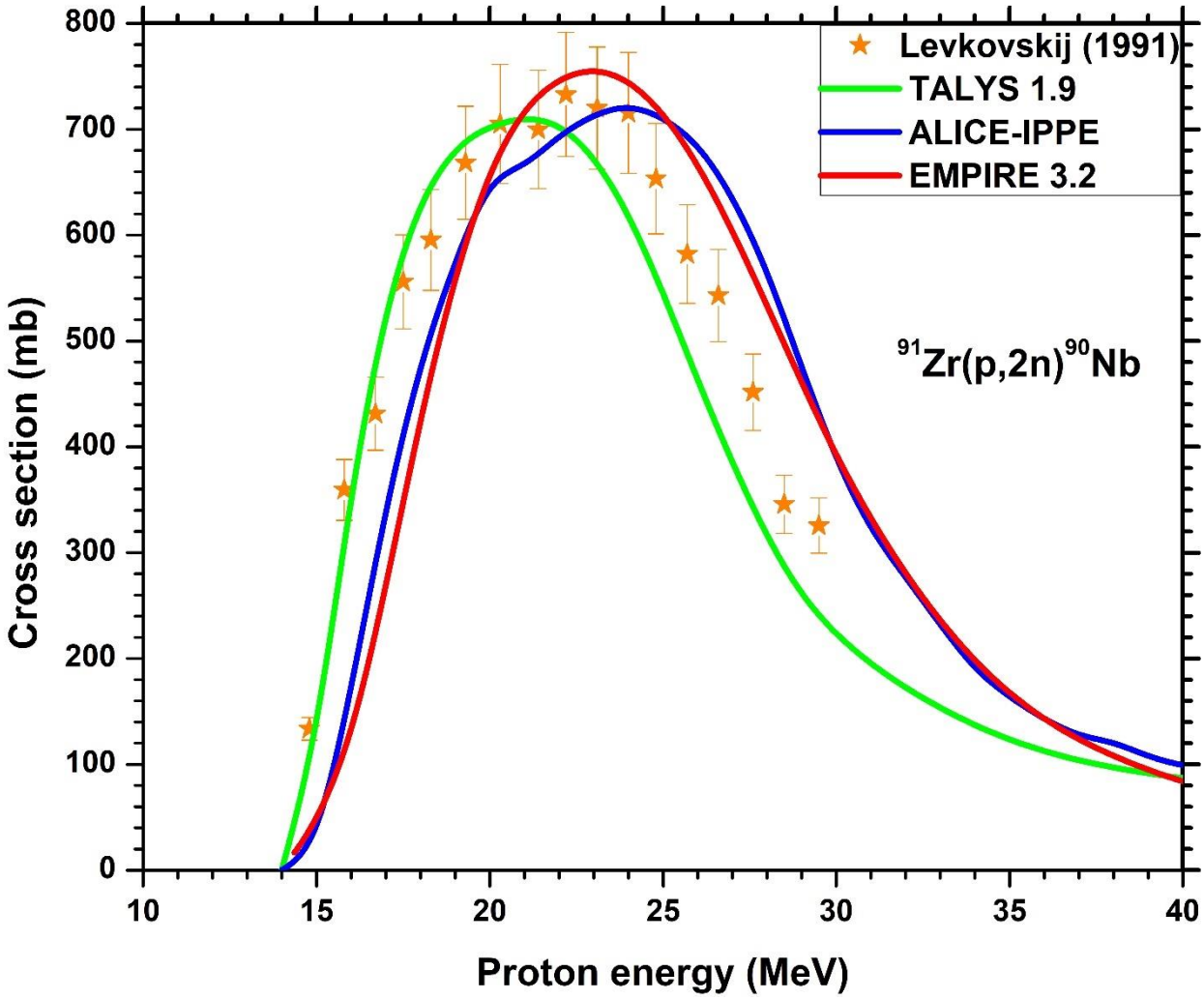

Figure 4 Normalized experimental data and results of nuclear model calculations for the $^{91}Zr(p,2n)^{90}Nb$ reaction

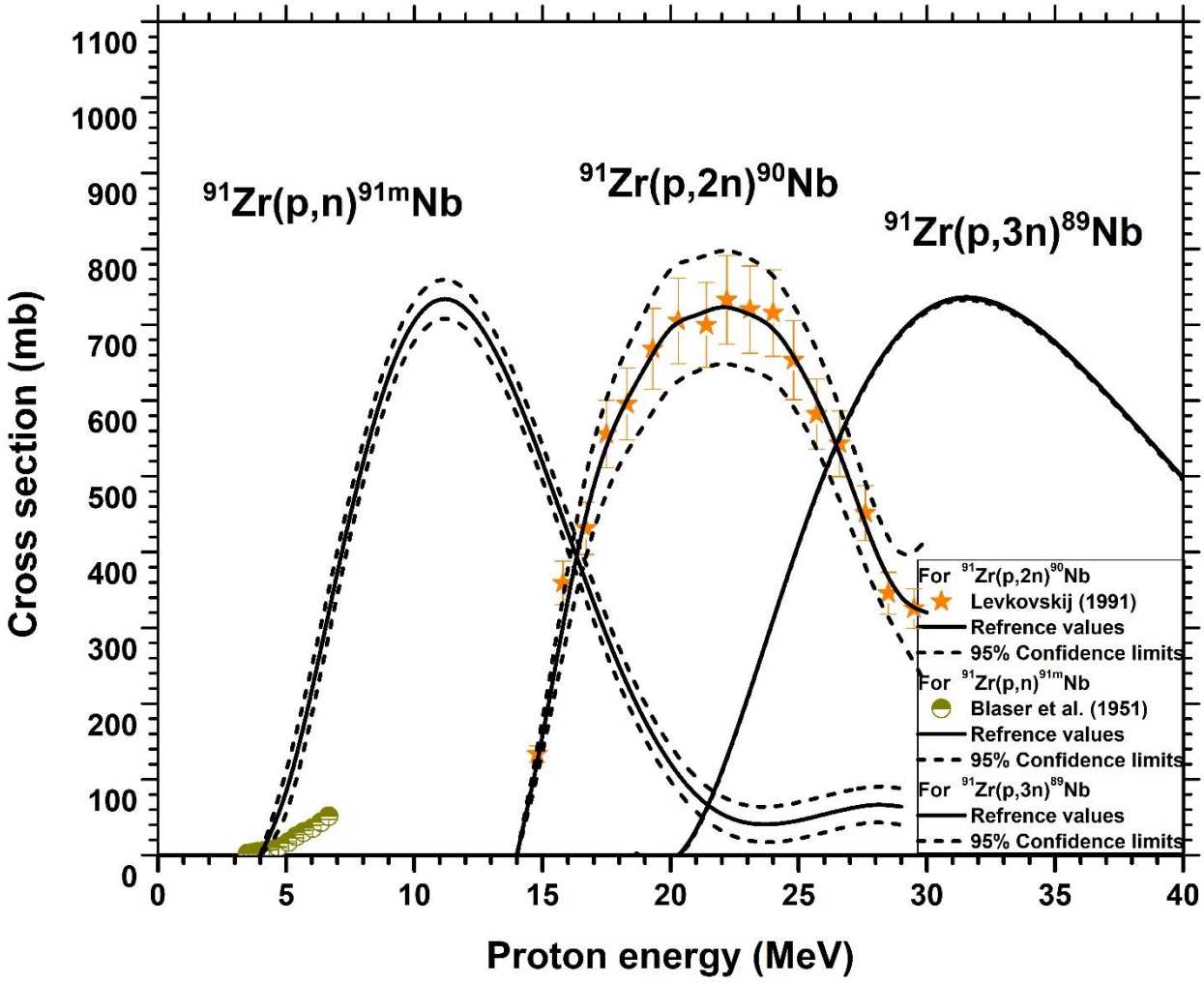

Figure 5 Selected experimental data and recommended cross section curve with 95% upper and lower confidence limits for the $^{91}Zr(p,2n)^{90}Nb$ reaction. The curves for ^{91m}Nb and ^{89}Nb are based on purely calculated cross sections.

3.1.3 $^{90}Zr(d,2n)^{90}Nb$

The database of this reaction is poor; only one author Mercader et al. (1972) has reported experimental values for this reaction (Table 1). They agree well with the results of nuclear model codes (Figure 6). As the results of all three nuclear model codes predicted well the entire excitation function so average of the theoretical results was taken as the reference value, shown in Figure 7.

Impurities

^{91m}Nb ($T_{1/2}$ = 60.86 d) and ^{89}Nb ($T_{1/2}$ = 2.03 h) are the two impurities that are produced via the reactions ^{90}Zr(d,n)^{91m}Nb and ^{90}Zr(d,3n)^{89}Nb, respectively. No data for ^{91m}Nb have been reported whereas for ^{89}Nb, only Usher et al. (1976) have reported a few data points which are insufficient for evaluation purposes. So, again we had to rely on the nuclear model calculations. The calculation of the (d,n) reaction via all the model codes is very uncertain due to deuteron breakup we therefore did not attempt it. The polynomial fitting of the theoretical data points was generated in order to obtain the reference values for ^{90}Zr(d,3n)^{89}Nb reaction (Figure 7).

Selected experimental data points and reference values along the 95% confidence limits for ^{90}Nb and ^{89}Nb are shown in Figure 7 whereas numerical values are given in Table 5.

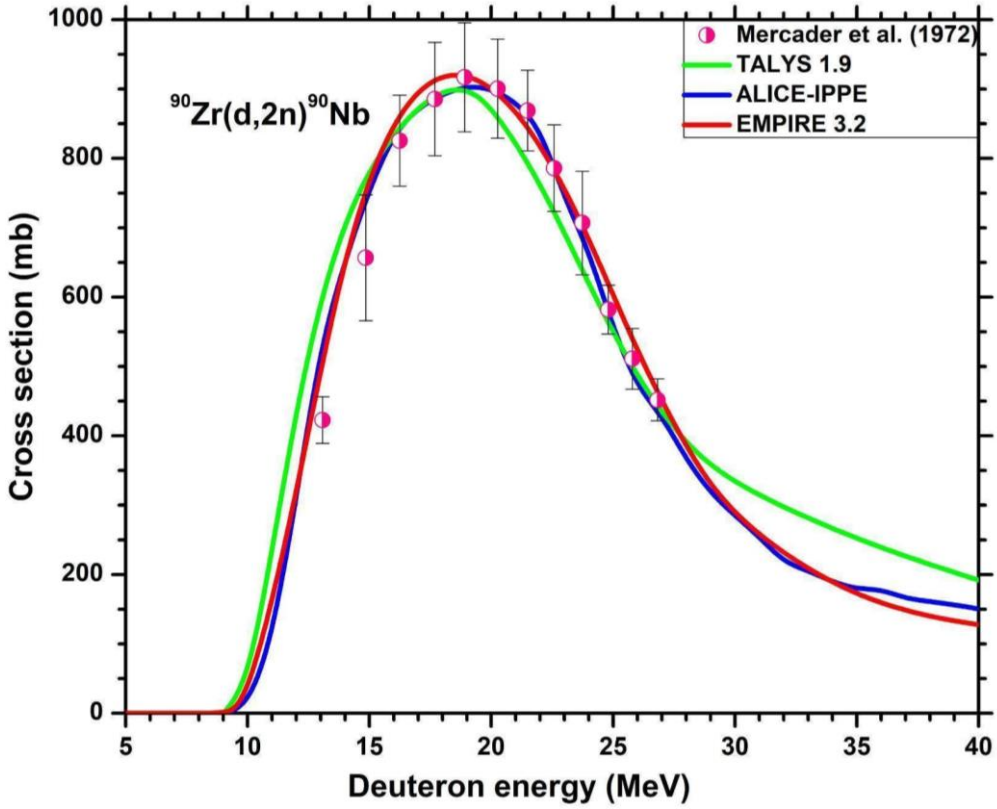

Figure 6 Normalized experimental data and results of nuclear model calculations for the ^{90}Zr(d,2n)^{90}Nb reaction

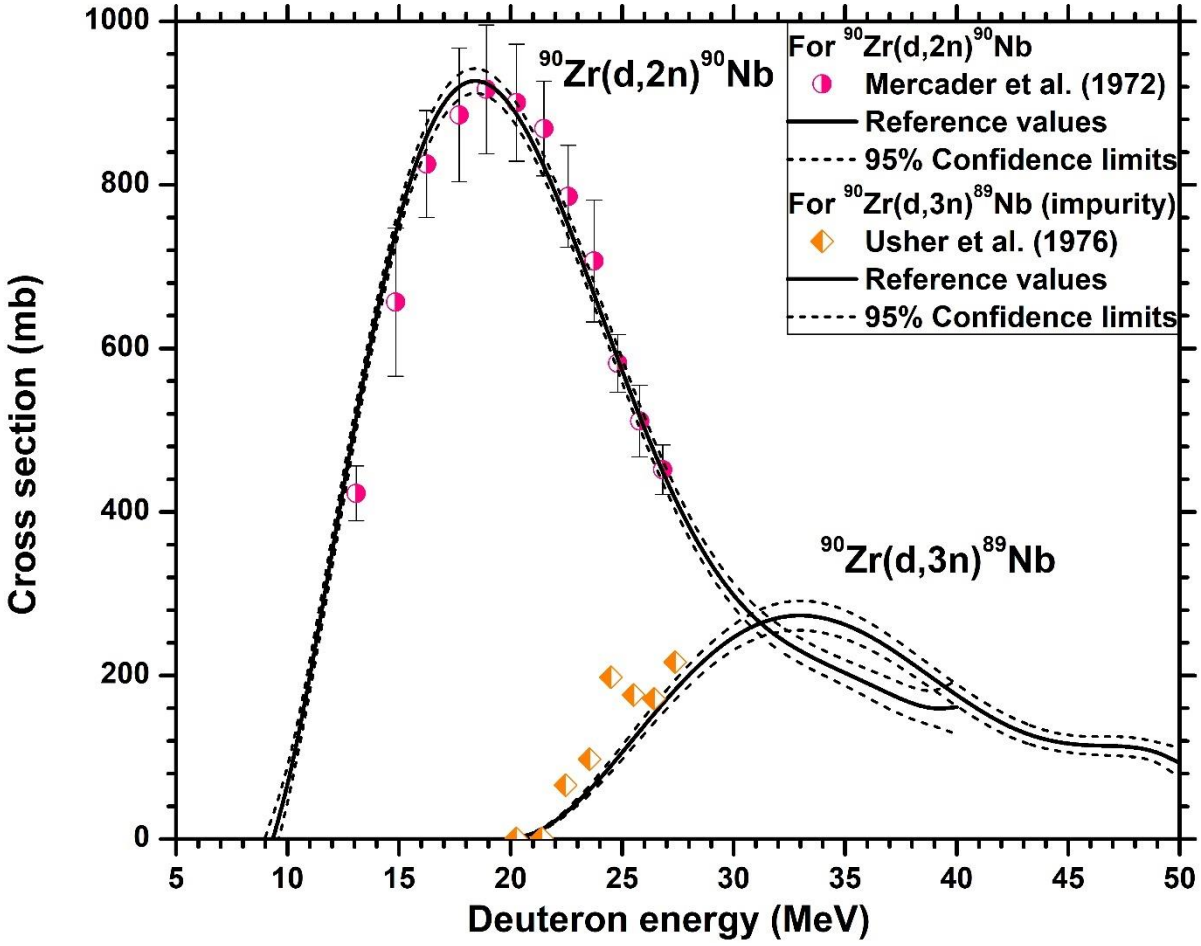

Figure 7 Selected experimental data and suggested cross section curve with 95% upper and lower confidence limits for ^{90}Zr(d,2n)^{90}Nb and ^{90}Zr(d,3n)^{89}Nb reactions.

3.2 Evaluation of production data of ^{90}Nb using ^{89}Y as target:

3.2.1 ^{89}Y(α,3n)^{90}Nb:

The database of this alpha-induced reaction is extensive but there is big scatter. In total seven authors, namely Chaubey et al. (1999), Levkovskij (1991), Singh et al. (2000), Smend et al. (1967), Murata et al. (2019), Mukherjee et al. (1997), and Shahid et al. (2015) reported data for this reaction. The data points reported by Mukherjee et al. (1997) and Murata et al. (2019) were normalized with a factor of 0.96 due to the difference of monitor cross sections with standard values.

The data points reported by Singh et al. (2000), Chaubey et al. (1999), and Smend et al. (1967) were discarded because of too low cross sections. All the available normalized experimental data points are shown in Figure 8 along with the results of the three nuclear model codes.

The datasets of Mukherjee et al. (1997), Levkovskij (1991), and Murata et al. (2019) are in better agreement with TALYS 1.9. Whereas the results of EMPIRE 3.2 nuclear model code are also in agreement with these data points till 42 MeV, thereafter, they underestimate the experimental values. The theoretically calculated values obtained using the ALICE-IPPE code slightly underestimate the experimental data till 45 MeV; afterwards, they overestimate the measured data.

Impurity

^{89}Nb occurs as an impurity, which is produced via the ^{89}Y(α,4n)^{89}Nb reaction. Murata et al. (2019), Shahid et al. (2015), and Chaubey et al. (1999) reported values for this reaction; however, they are inconsistent and cannot be used for evaluation. As a result, we again relied on the results of theoretical model calculations. After taking an average of those results, a polynomial fitting was performed on the average in order to obtain the recommended fit (Figure 9).

The above-mentioned evaluation methodology was utilized to generate the recommended fit. Selected experimental data points along with the recommended fit with 95% confidence limits for both ^{90}Nb and ^{89}Nb are shown in Figure 9 whereas their numerical values are given in Table 6.

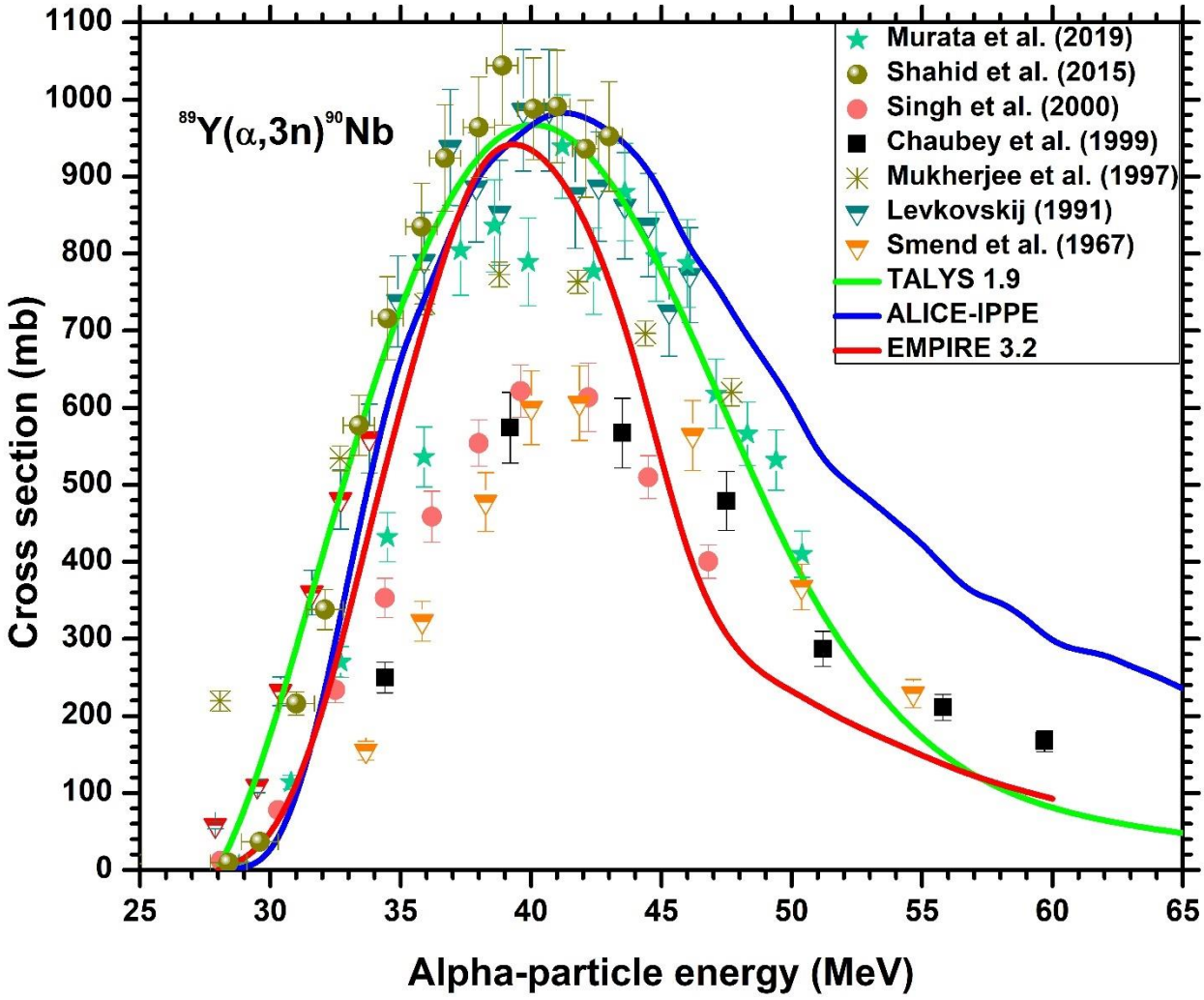

Figure 8 Normalized experimental data and results of nuclear model calculations for the ^{89}Y(α,3n)^{90}Nb reaction

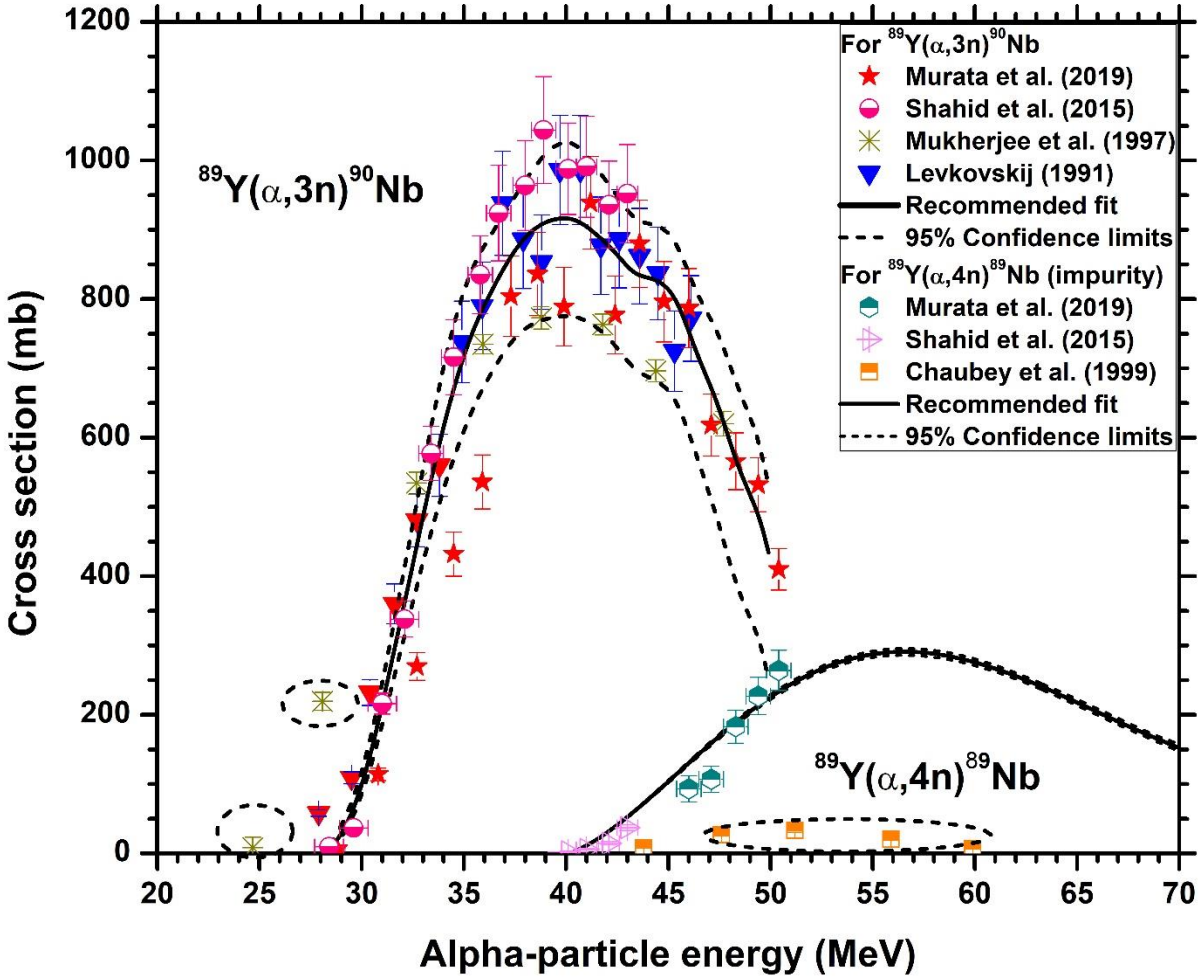

Figure 9 Selected experimental data and recommended cross section curve with 95% upper and lower confidence limits for the ^{89}Y(α,3n)^{90}Nb and ^{89}Y(α,4n)^{89}Nb reactions. Encircled data points are discarded.

Impurity

^{91m}Nb *($T_{1/2}$= 60.9 d)* also occurs acts as a radioisotopic impurity, formed via the ^{89}Y(α,2n)^{91m}Nb reaction. Two authors, i.e. Murata et al. (2019) and Shahid et al. (2015), reported values for this reaction. Both of these data sets are in better agreement with each other. The above-mentioned evaluation methodology is utilized for calculating the recommended fit for this reaction (shown in Figure 10).

^{92m}Nb ($T_{1/2}$= 10.15 d) is another significant impurity that is formed via the ^{89}Y(α,n)^{92m}Nb reaction. For this reaction, six authors reported the measured cross sections. The data points reported by Mukherjee et al. (1997) were normalized by a factor of 3% on the basis of monitor

reaction; however, it is still much higher than the other data sets that's why it was discarded. All other experimental data points and the recommended fit are shown in Figure 10.

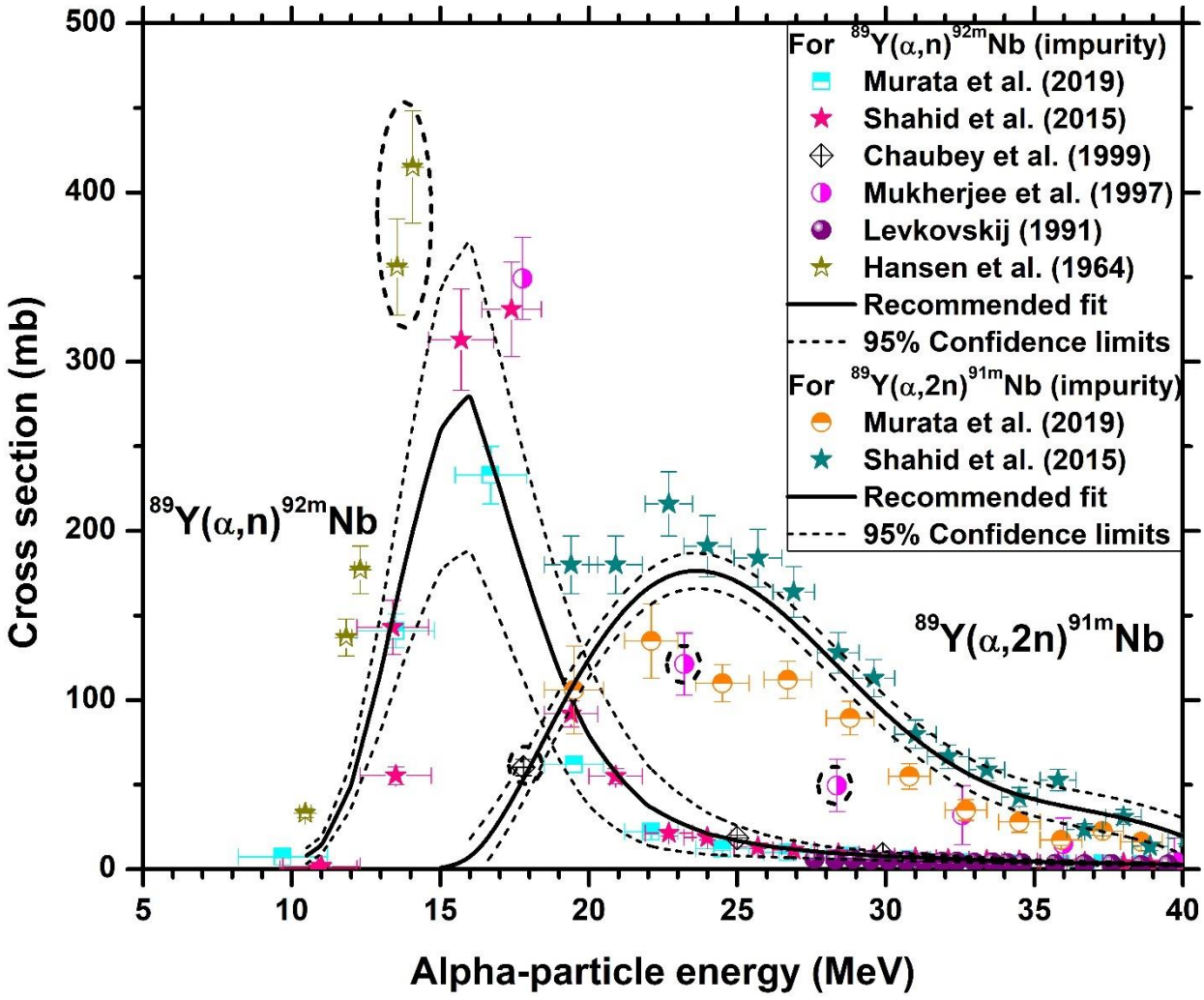

Figure 10 Normalized experimental data and recommended cross section curve with 95% upper and lower confidence limits for the $^{89}Y(\alpha,n)^{92m}Nb$ and $^{89}Y(\alpha,2n)^{91m}Nb$ reactions. Encircled data points are discarded.

3.3 Evaluation of production data of ^{90}Nb using ^{93}Nb target:

3.3.1 $^{93}Nb(p,4n)^{90}Mo\rightarrow^{90}Nb$:

The nuclear process $^{93}Nb(p,4n)^{90}Mo\rightarrow^{90}Nb$ is an indirect route for the production of ^{90}Nb. After the formation of ^{90}Mo it chould be separated radiochemically, then allowed to decay to ^{90}Nb, which could then be further separated radiochemically. So the decay of ^{90}Mo would give high purity product ^{90}Nb. This was practically shown by (Butement and Qaim, 1964)). The work was, however, only qualitative and no cross sections or yields were measured. Regarding the

latter, a total of six authors have reported their measurements for this reaction. Experimental data and the results of the theoretical model calculations are shown in Figure 11. In comparison to the results reported by Ditroi et al. (2008), the other data points are in a better agreement with one another. The theoretical calculations obtained using the three nuclear model codes do not adequately predict the excitation function. The evaluation methodology described above was used to generate the recommended fit which is depicted in Figure 12 whereas numerical values are given in Table 7.

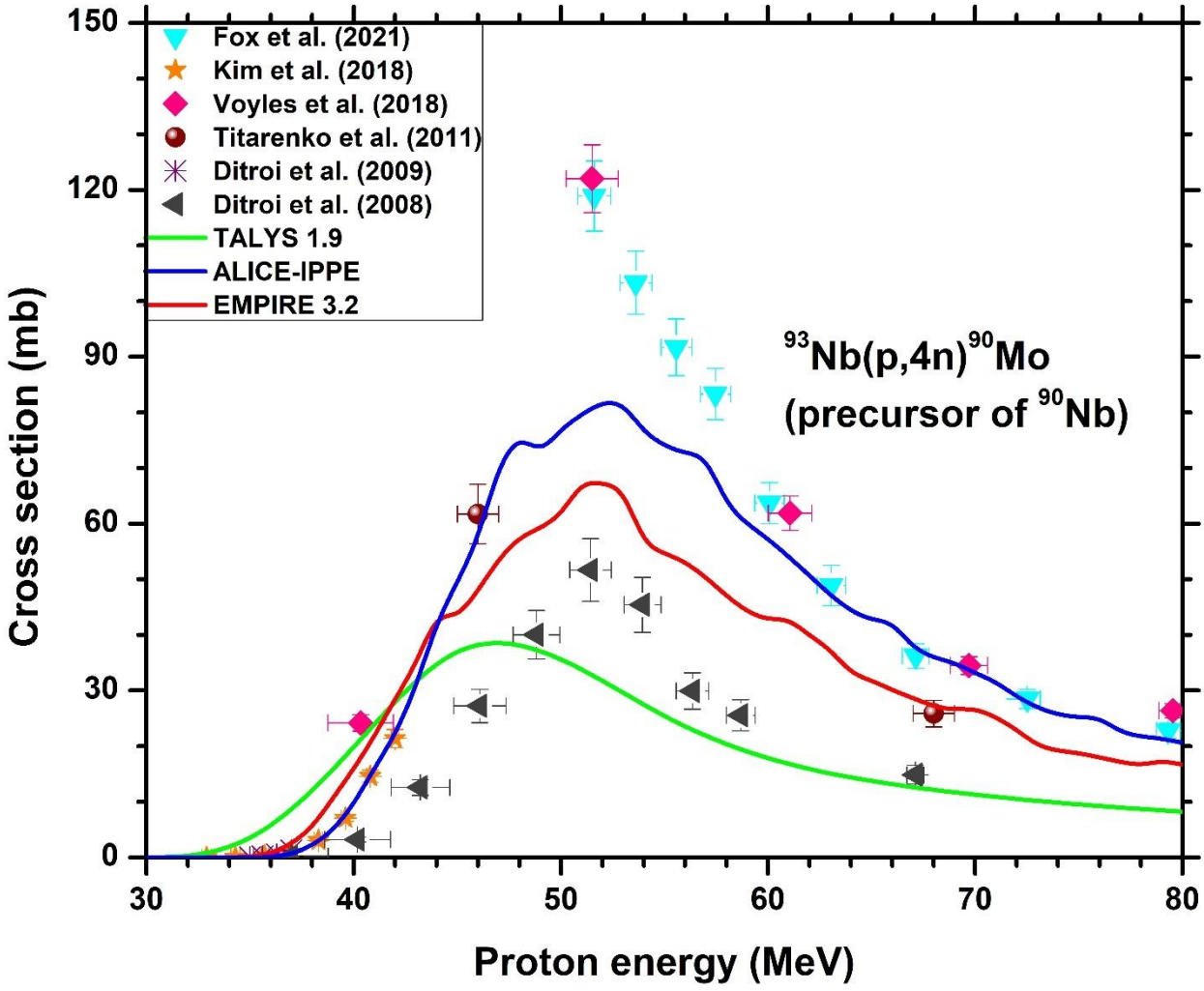

Figure 11 Normalized experimental data and theoretical curves for the ^{93}Nb(p,4n)^{90}Mo reaction.

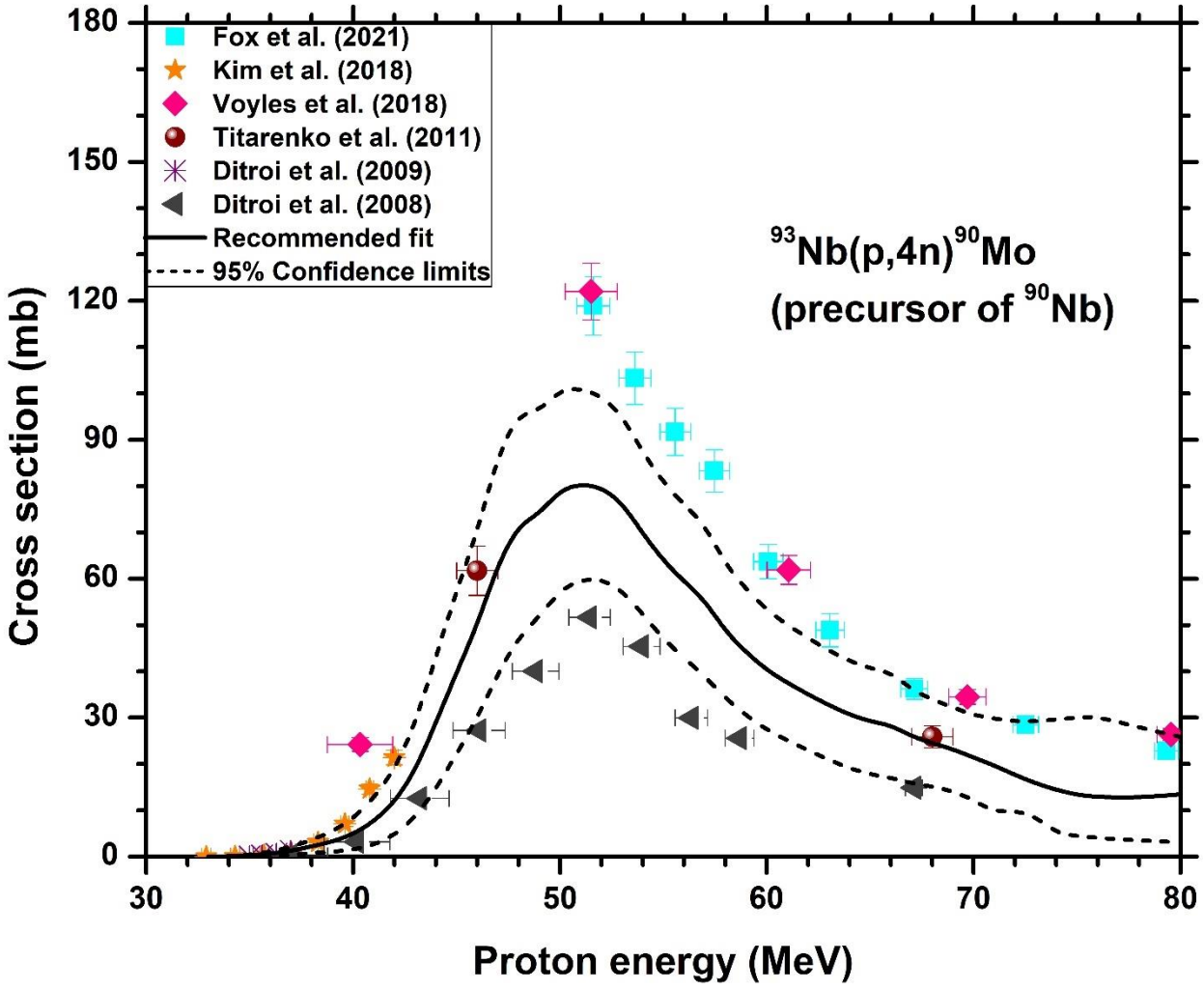

Figure 12 Normalized experimental data and recommended cross section curve with 95% upper and lower confidence limits for the ^{93}Nb(p,4n)^{90}Mo reaction.

4 Validation of evaluated cross sections

For neutron induced reactions, there are some very well-defined benchmarks for the validation of evaluated data, for example, a reactor neutron spectrum (Uddin et al., 2013) or a 15 MeV d/Be neutron spectrum (Al-Abyad et al., 2006). However, the methodology for the validation of evaluated data of charged particle induced reactions is not established yet. One approach is to measure integral yield under certain defined conditions (Kastleiner et al., 2002; Qaim et al., 2007). The other approach for validating the evaluated data is the normalization of the enriched target isotopes based on the natural isotopic composition of the target element and then comparing it with the experimentally measured cross sections for the natural element (Aslam

et al., 2015). This approach is quite effective in throwing light on the quality of evaluated data; however, it does not replace the need for some well-planned measurements.

Natural Zirconium consists of five isotopes of different abundances (i.e., ^{90}Zr (51.45%), ^{91}Zr (11.22%), ^{92}Zr (17.15%), ^{94}Zr (17.38%), and ^{90}Zr (2.80%)). The evaluated data from this work were validated by comparison with the measurements for the ^{nat}Zr(p,x)^{90}Nb.

4.1 ^{nat}Zr(p,x)^{90}Nb

Several authors have used ^{nat}Zr as a target for the production of ^{90}Nb via the reaction ^{nat}Zr(p,x)^{90}Nb (Uddin et al., 2008; Al-Abyad et al., 2009; Khandaker et al., 2009; Murakami et al., 2014; Szelecsényi et al., 2015; Tárkányi et al., 2015; Lawriniang et al., 2018; Yang et al., 2018). All available experimental cross section data along with the evaluated data curve obtained by normalizing the evaluated cross sections of ^{90}Zr(p,n)^{90}Nb and ^{91}Zr(p,2n)^{90}Nb reactions is shown in Figure 13. The data reported by Lawriniang et al. (2018), Yang et al. (2018), Szelecsenyi et al. (2015), Tarkanyi et al. (2015), Murakami et al. (2014), and Khandaker et al. (2009) appear to be in a reasonable agreement with the normalized data curve. The data points reported by Uddin et al. (2008) are also show a reasonable agreement apart from the first two data points. The data reported by Al-abyad et al. (2012) are slightly higher than the normalized curve above 13 MeV.

Overall seen, apart from some discrepant measurements, the trend of the majority of data is very well described by our normalized curve from the evaluated data. Hence, it is concluded that the recommended fits given in our work for the ^{90}Zr(p,n)^{90}Nb and ^{91}Zr(p,2n)^{90}Nb reactions are well validated through the comparison with measurements on ^{nat}Zr as a target material.

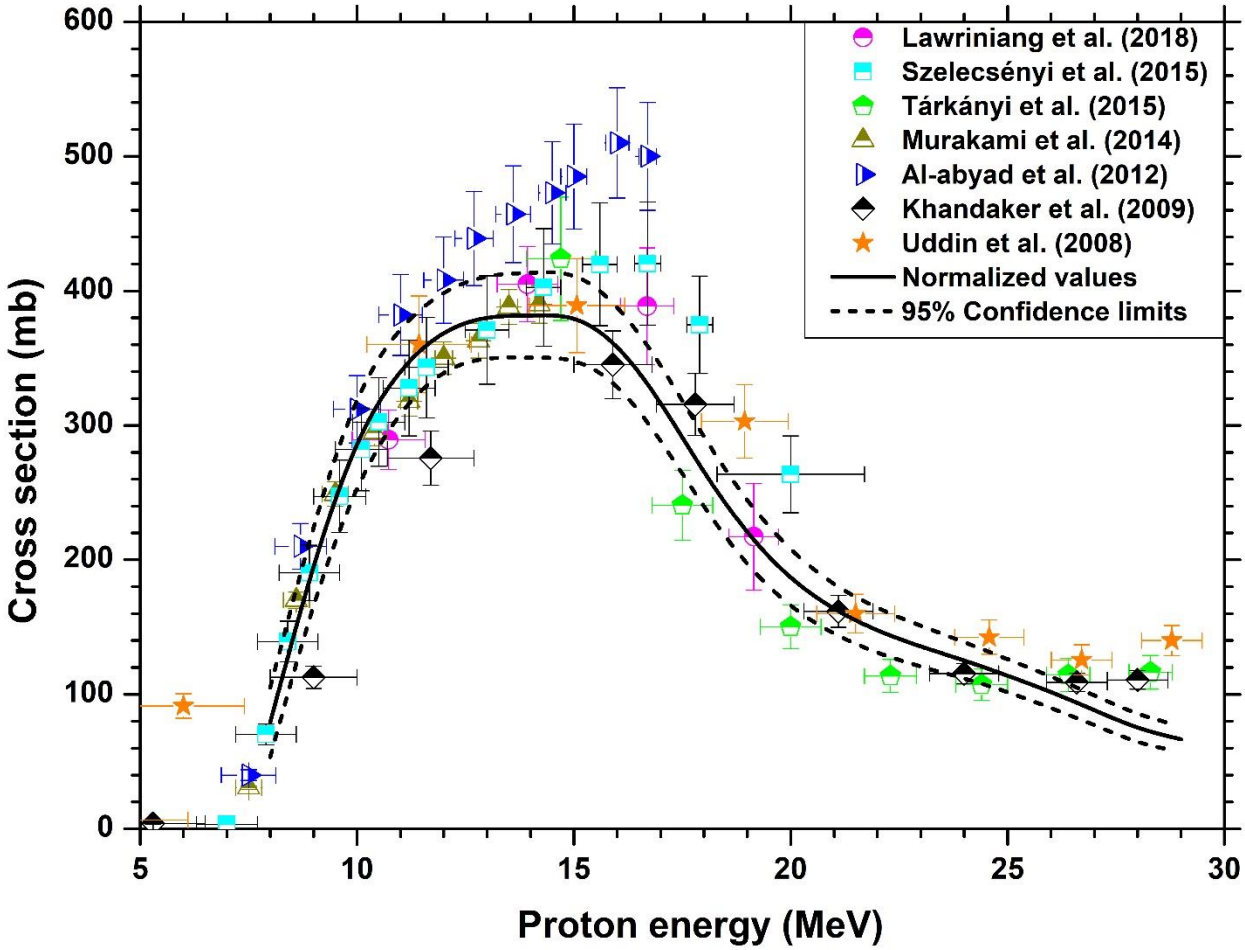

Fig 13. Experimental data and evaluated curve for $^{nat}Zr(p,x)^{90}Nb$ reaction. The solid curve is based on a normalization of the evaluated data of the $^{90}Zr(p,n)^{90}Nb$ and $^{91}Zr(p,2n)^{90}Nb$ reactions to ^{nat}Zr as target.

5 Calculation and comparison of thick target yields

Thick target yields of ^{90}Nb were calculated by using the fitted cross sections and the standard formula (Qaim, 1982) for an irradiation time of 1h and a beam current of 1μ**A** (Otuka and Takacs, 2015). These yields serve as a benchmark for the highest possible value that can be attained in an experiment. Figures 15-18 show the thick target yields for the $^{90}Zr(p,n)^{90}Nb$, $^{91}Zr(p,2n)^{90}Nb$, $^{90}Zr(d,2n)^{90}Nb$, $^{89}Y(\alpha,3n)^{90}Nb$, and $^{93}Nb(p,4n)\ ^{90}Mo$ reactions, respectively, assuming 100% enrichment of each target. In order to conduct a comprehensive impurity analysis, the thick target yields for the corresponding impurity reactions $^{90}Zr(p,2n)^{89}Nb$, $^{91}Zr(p,3n)^{89}Nb$, $^{91}Zr(p,n)^{91m}Nb$, $^{90}Zr(d,3n)^{89}Nb$, $^{89}Y(\alpha,n)^{92m}Nb$, $^{89}Y(\alpha,2n)^{91m}Nb$, and $^{89}Y(\alpha,4n)^{89}Nb$ were also calculated and are shown in Figures 15-18, respectively.

5.1.1 Thick target yields of ^{90}Zr(p,n)^{90}Nb and ^{90}Zr(p,2n)^{89}Nb reactions

The ^{90}Zr(p,n)^{90}Nb reaction is a potential route for clinical scale production of ^{90}Nb. Using the data obtained from the fitted curve, the thick target yields of the ^{90}Zr(p,n)^{90}Nb and ^{90}Zr(p,2n)^{89}Nb reactions were computed; these values are shown in Figure 14. Three authors (Nickles, 1991; Busse et al., 2002; Radchenko et al., 2014) reported the experimentally yield values for the ^{90}Zr(p,n)^{90}Nb reaction. The values reported by Busse et al. (2002) almost exactly the same as our calculated yield values whereas Nickles (1991) reported a yield of 1628 MBq/μAh at 11 MeV, which is much higher than our calculated values. The yield reported by Radchenko et al. (2014) for E_p=17.5→13 MeV and a current of 5μA when normalized to 100% ^{90}Zr, amounts to about 300 MBq/μAh. This value is comparable to our theoretical value of 340 MBq/μAh.

By comparing the production route of the desired products, e.g., ^{90}Nb or ^{89}Nb, it can be easily noticed from Figure 15 that the production rate of ^{89}Nb increases after 16 MeV. So, 100% pure ^{90}Nb can be produced, by selecting the energy range between 16→8 MeV. Our calculated integral yield for ^{90}Nb in our energy range is 482 MBq/μAh.

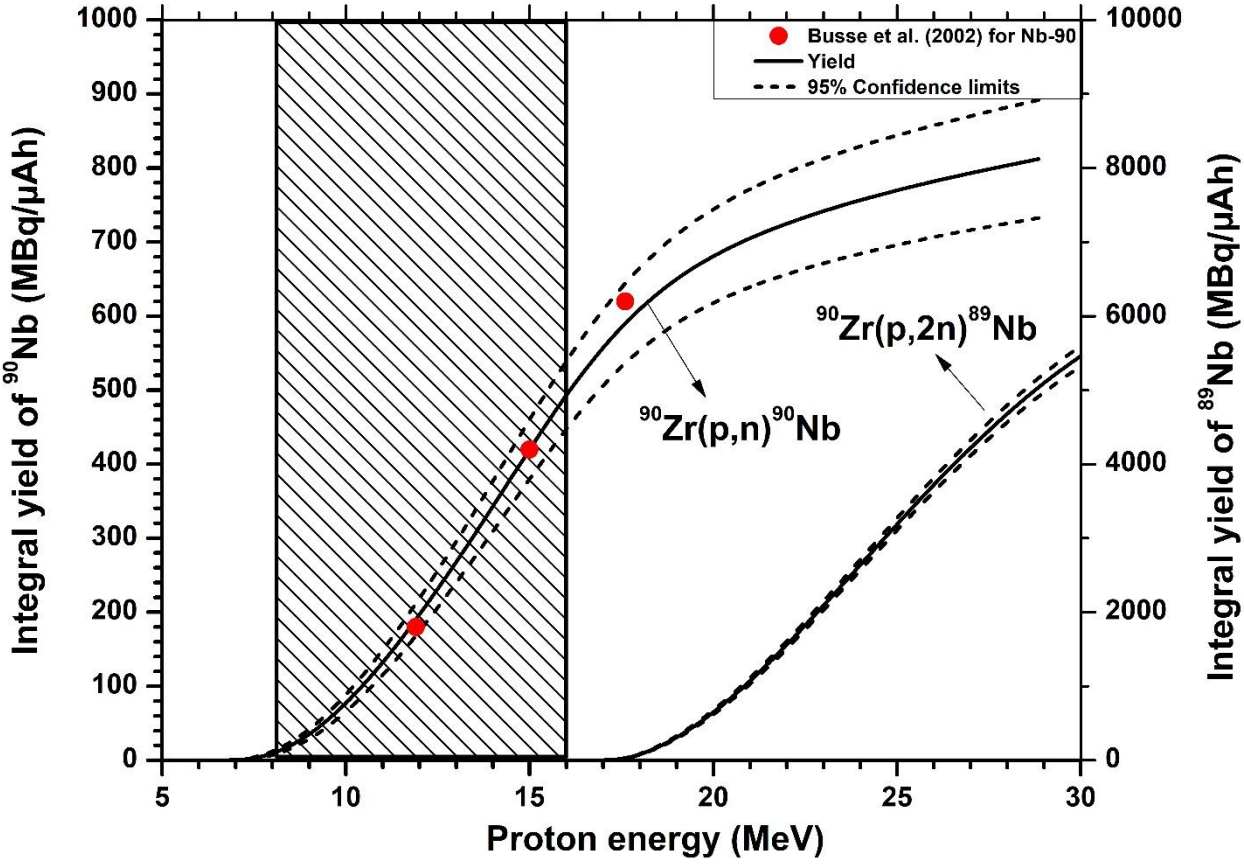

Figure 14 Integral yields of the ^{90}Zr(p,n)^{90}Nb and ^{90}Zr(p,2n)^{89}Nb reactions calculated from our evaluated curves, and comparison with the experimentally determined thick target yields of ^{90}Nb by Busse et al. (2002)

5.1.2 Thick target yields of ^{91}Zr(p,2n)^{90}Nb and ^{91}Zr(p,3n)^{89}Nb

^{91}Zr(p,2n)^{90}Nb also has the potential to be used as an effective production route of ^{90}Nb. The calculated thick target yields of both ^{91}Zr(p,2n)^{90}Nb and ^{91}Zr(p,3n)^{89}Nb reactions are shown in Figure 15. After the analysis, an energy window of E_p = 24→15 MeV is suggested for the high purity production of ^{90}Nb. In this energy region, our calculated yield is 747 MBq/μAh with no contribution from the impurity reaction ^{91}Zr(p,3n)^{89}Nb.

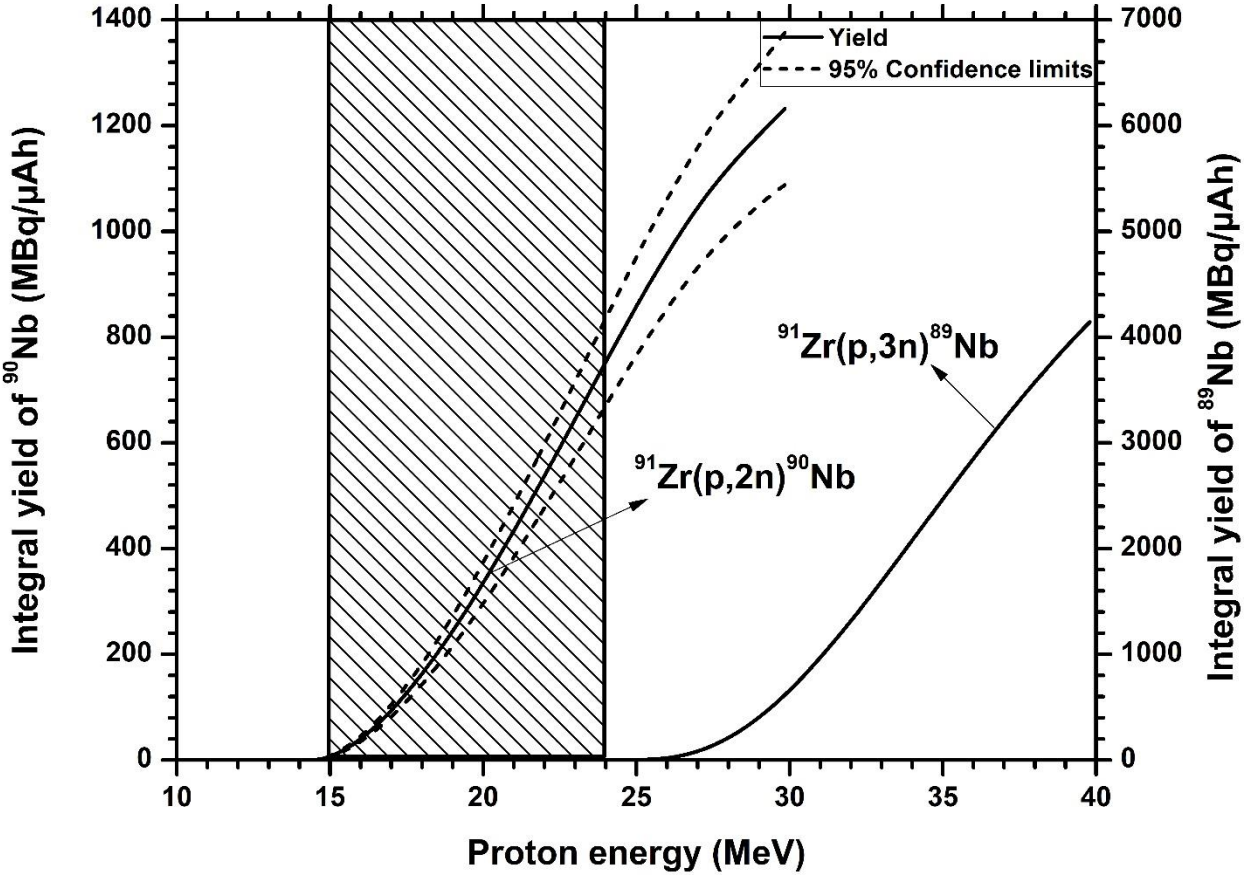

Figure 15 Calculated integral yields of the ^{91}Zr(p,2n)^{90}Nb and ^{91}Zr(p,3n)^{89}Nb reactions.

5.1.3 Thick target yields of ^{90}Zr(d,2n)^{90}Nb and ^{90}Zr(d,3n)^{89}Nb reactions

The calculated integral yield of the ^{90}Zr(d,2n)^{90}Nb reaction and of the contributing impurity ^{90}Zr(d,3n)^{89}Nb reaction are shown in Figure 16. The production rate of ^{89}Nb increases from 20 MeV onwards. So, we suggest an energy region of E_d = 21→12 MeV for 100% pure production of ^{90}Nb. In this region, our calculated integral yield is 519 MBq/μAh. This value is comparable

to that via the $^{90}Zr(p,n)^{90}Nb$ route discussed above. The higher energy range needed for the $^{90}Zr(d,2n)^{90}Nb$ reaction is however, somewhat disadvantageous.

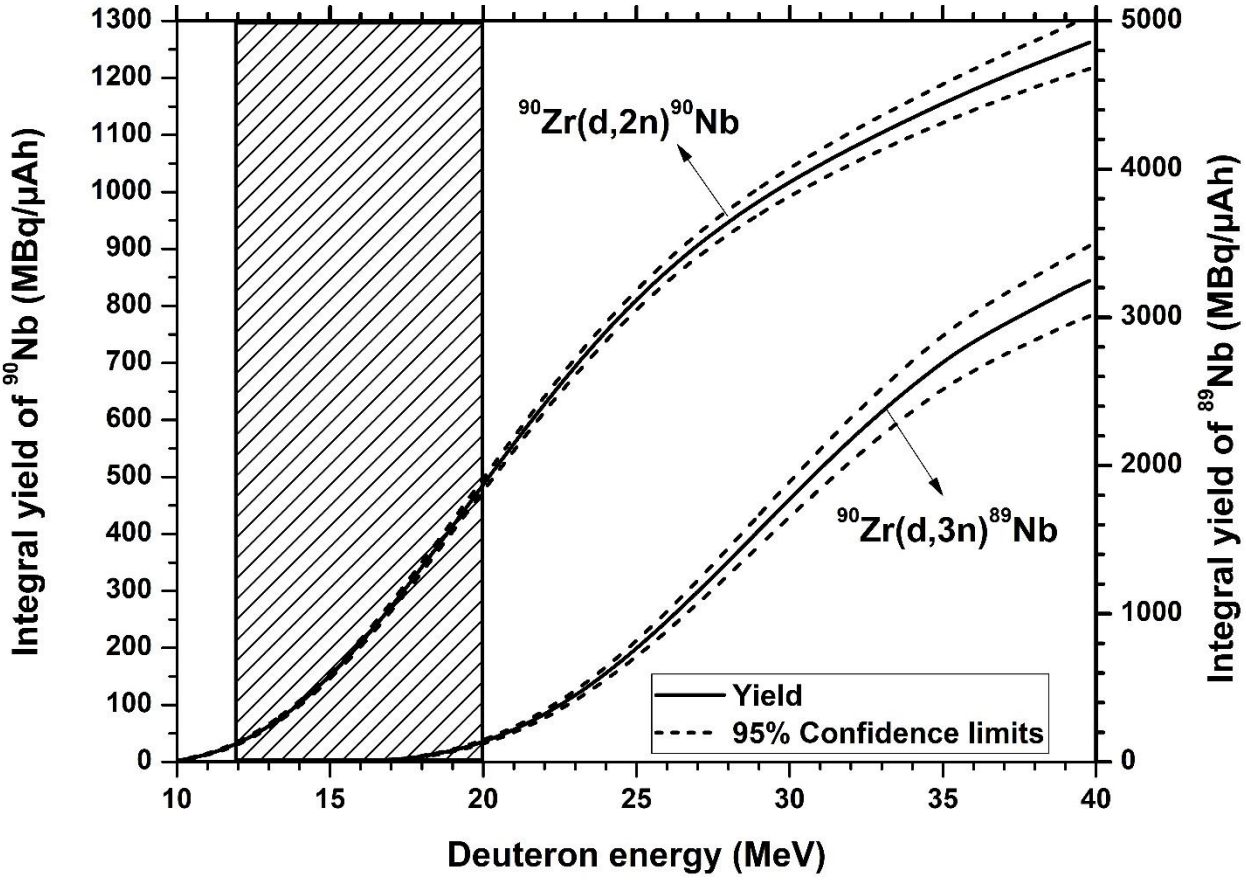

Figure 16 Calculated integral yields of the $^{90}Zr(d,2n)^{90}Nb$ and $^{90}Zr(d,3n)^{89}Nb$ reactions.

5.1.3 Thick target yields of $^{89}Y(\alpha,3n)^{90}Nb$ and $^{89}Y(\alpha,4n)^{89}Nb$ reactions

The calculated integral yields of the $^{89}Y(\alpha,3n)^{90}Nb$ and $^{89}Y(\alpha,4n)^{89}Nb$ reactions are shown in Figure 17. No experimental yield value for these reactions has been reported. The impurity reactions namely $^{89}Y(\alpha,n)^{92m}Nb$ and $^{89}Y(\alpha,2n)^{91m}Nb$ have negligible yields as compared to $^{89}Y(\alpha,3n)^{90}Nb$ and $^{89}Y(\alpha,4n)^{89}Nb$ reactions; therefore they are not shown in the figure. After analysis, an energy region $E_\alpha = 39 \rightarrow 31$ MeV was selected for the high purity production of ^{90}Nb. In the suggested region our calculated integral yield is 53 MBq/μAh.

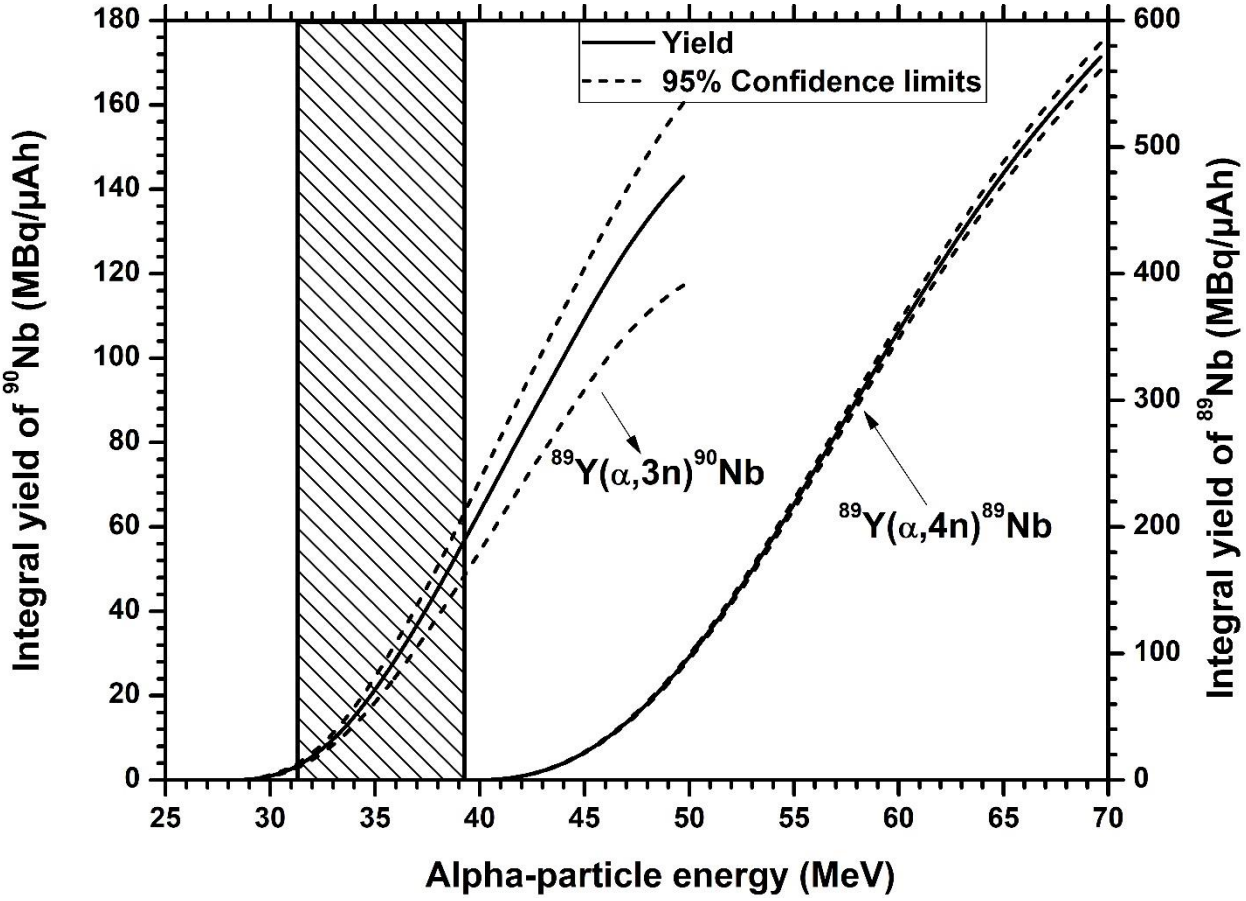

Figure 17 Calculated integral yields of the ^{89}Y(α,3n)^{90}Nb and ^{89}Y(α,4n)^{89}Nb reactions

5.2 Comparison of production routes

The production rates of ^{90}Nb via all evaluated routes, namely ^{90}Zr(p,n)^{90}Nb, ^{91}Zr(p,2n)^{90}Nb, ^{90}Zr(d,2n)^{90}Nb, and ^{89}Y(α,3n)^{90}Nb, are compared in Figure 18. Both ^{90}Zr(p,n)^{90}Nb and ^{91}Zr(p,2n)^{90}Nb reactions give higher integral yields than the deuteron and the alpha-particle induced reactions. The production route ^{90}Zr(p,n)^{90}Nb is suitable for high-purity production at low energy cyclotrons, whereas the reactions ^{91}Zr(p,2n)^{90}Nb and ^{90}Zr(d,2n)^{90}Nb are suitable for the production of ^{90}Nb at medium energy cyclotrons.

The remaining production routes, namely ^{89}Y(α,3n)^{90}Nb and ^{93}Nb(p,4n)^{90}Mo→^{90}Nb, give high purity product at higher energies but comparatively with lower integral yield values than the (p,n) and (p,2n) reactions on ^{90}Zr and ^{91}Zr respectively. Furthermore, in case of the ^{89}Y(α,3n)^{90}Nb reaction, the contribution of radionuclidic impurity becomes significant with increasing energies. Only ^{93}Nb(p,4n)^{90}Mo→^{90}Nb reaction is suitable for high energy cyclotron production of 100% pure ^{90}Nb. It gives integral yield of 440 MBq/μAh (calculated) in an energy region E_p = 80→40 MeV.

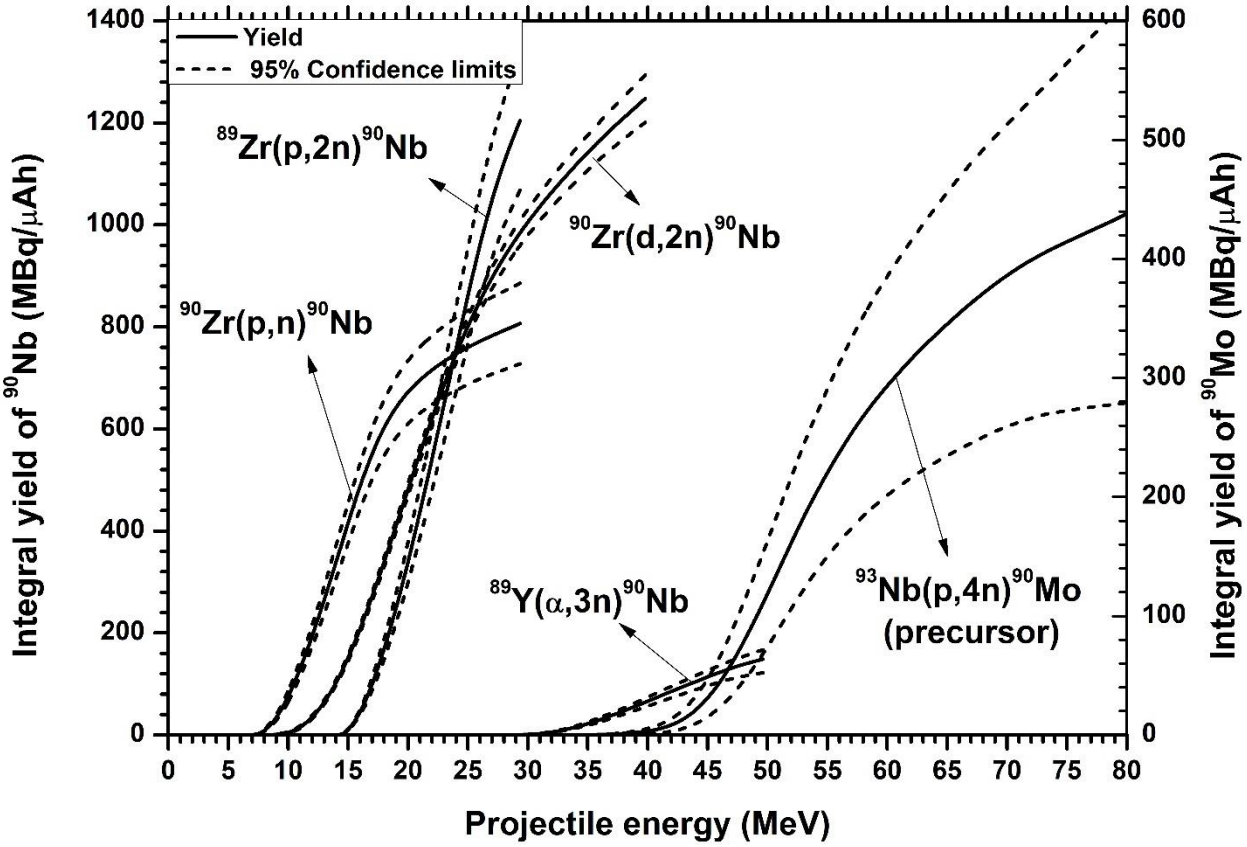

Figure 18 Comparison of production routes of ^{90}Nb on the basis of their integral yields as well integral yield of the precursor ^{90}Mo.

6 Conclusions:

We have evaluated five production routes, namely $^{90}Zr(p,n)^{90}Nb$, $^{91}Zr(p,2n)^{90}Nb$, $^{90}Zr(d,2n)^{90}Nb$, $^{89}Y(\alpha,3n)^{90}Nb$ and $^{93}Nb(p,4n)^{90}Mo\rightarrow^{90}Nb$, for the production of the non-standard positron emitter ^{90}Nb. For each production route the reliability of the experimental data was critically analyzed on the basis of three nuclear model calculations, then a well-developed evaluation methodology was used to generate the recommended cross sections. The same procedure was adopted for the evaluation of contributing impurity reactions. A reference curve was given where experimental data were insufficient for evaluation. Using the recommended cross sections, thick target yields were calculated, and optimum ranges are suggested for high purity production of ^{90}Nb. Numerical values of Integral yields in the suggested energy regions with the percentage level of contributing radionuclidic impurities are given in Table 8.

The reaction $^{90}Zr(p,n)^{90}Nb$ gives an integral yield of 482 MBq/μAh in an energy range of $16\rightarrow8$ MeV; it is a suitable production route for small cyclotrons. The reactions $^{91}Zr(p,2n)^{90}Nb$ and $^{90}Zr(d,2n)$ give higher production rates with an integral yield of 747 MBq/μAh and 519 MBq/μAh in the energy range of $E_p=24\rightarrow15$ MeV and $E_d=21\rightarrow12$ MeV respectively. These reactions are suitable for medium energy cyclotron production of ^{90}Nb but experimental data in literature is not sufficient for their confident evaluation. The production route $^{89}Y(\alpha,3n)^{90}Nb$ is a less convenient choice due its low integral yield (53 MBq/μAh) in high energy range of $E_\alpha=39\rightarrow31$ MeV.

The reaction $^{93}Nb(p,4n)^{90}Mo\rightarrow^{90}Nb$ gives high purity production of ^{90}Nb and gives integral yield value of 440 MBq/μAh in the energy range of $E_p=80\rightarrow40$ MeV. This is a method of choice for 100% pure production of ^{90}Nb using high energy cyclotrons.

After a careful analysis based on the comparison of production routes and level of radioisotopic impurities, it is concluded that the $^{90}Zr(p,n)^{90}Nb$ reaction is the most suitable production route of ^{90}Nb at low energy cyclotrons. The normalized recommended cross sections for $^{90}Zr(p,n)^{90}Nb$ and $^{91}Zr(p,2n)^{90}Nb$ reactions were also validated by comparison with the $^{nat}Zr(p,x)^{90}Nb$ reaction. So, our recommended cross section values can be confidently used for the high purity production of the radioisotope ^{90}Nb. In fact for real clinical scale production of ^{90}Nb, so far only the $^{90}Zr(p,n)^{90}Nb$ reaction has been successfully applied.

9 Acknowledgments

N. Amjed would like to thank the Higher Education Commission of Pakistan (HEC) for the financial assistance. The work was done in the frame of HEC; NRPU project No. 9746.

References:

Al-Abyad, M., Comsan, M.N.H., Qaim, S.M., 2009. Excitation functions of proton-induced reactions on ^{nat}Fe and enriched ^{57}Fe with particular reference to the production of ^{57}Co. Appl. Radiat. Isot. 67, 122-128.

Al-Abyad, M., Spahn, I., Sudár, S., Morsy, M., Comsan, M.N.H., Csikai, J., Qaim, S.M., Coenen, H.H., 2006. Nuclear data for production of the therapeutic radionuclides ^{32}P,^{64}Cu,^{67}Cu,^{89}Sr,^{90}Y and ^{153}Sm via the (n,p) reaction: Evaluation of excitation function and its validation via integral cross-section measurement using a 14 MeV d(Be) neutron source. Appl. Radiat. Iso. 64, 717-724.

Amjed, N., Aslam, M.N., Hussain, M., Qaim, S.M., 2021. Evaluation of nuclear reaction cross section data of proton and deuteron induced reactions on ^{75}As, with particular emphasis on the production of ^{73}Se. Radiochim. Acta 105, 525-537.

Amjed, N., Naz, A., Wajid, A.M., Aslam, M.N., Ahmad, I., 2022. Nuclear model analysis and optimization of production data of the medically interesting ^{66,67,68}Ga via alpha induced reactions on ^{63,65}Cu targets. Appl. Radiat. Isot. 188, 0969-8043.

Aslam, M.N., Sudár, S., Hussain, M., Malik, A.A., Shah, H.A., Qaim, S.M., 2010. Evaluation of excitation functions of proton and deuteron induced reactions on enriched tellurium isotopes with special relevance to the production of iodine-124. Appl. Radiat. Isot. 68, 1760-1773.

Aslam, N., Amjed, N., Qaim, S.M., 2015. Evaluation of excitation functions of the ^{68,67,66}Zn(p,xn)^{68,67,66}Ga and ^{67}Zn(p,α)^{64}Cu reactions: validation of evaluated data through comparison with experimental excitation functions of the ^{nat}Zn(p,x)^{66,67}Ga and ^{nat}Zn(p,x)^{64}Cu processes. Appl. Radiat. Isot. 96, 102-113.

Biryukov, N.S., Zhuravlev, B.V., Rudenko, A.P., Sal'nikov, O.A., Trykova, V.I., 1980. Direct and equilibrium processes in (p,n) reactions at a proton energy 22.2 MeV. Sov. J. Nucl. Phys. 31, 291-294.

Blaser, J.P., Boehm, F., Marmier, P., Scherrer, P., 1951. Excitation functions and cross sections of the (p,n) reaction. II. Helvet. Phys. Acta 24, 1-37.

Bojowald, J., Machner, H., Nann, H., Oelert, W., Rogge, M., Turek, P., 1988. Elastic deuteron scattering and optical model parameters at energies upto100 MeV. Phys. Rev. C 38, 1153-1163.

Boswell, C.A., Brechbiel, M.W., 2007. Development of radioimmunotherapeutic and diagnostic antibodies: an inside-out view. Nucl. Med. Bio. 34, 757-778.

Busse, S., Rösch, F., Qaim, S.M., 2002. Cross section data for the production of the positron emitting niobium isotope ^{90}Nb via the ^{90}Zr (p,n)-reaction. Radiochim. Acta 90, 1-5.

Butement, F.D.S., Qaim, S.M., 1964. New radioisotopes of niobium and molybdenum—II ^{88}Mo and ^{89}Mo. J. Inorg. Nucl. Chem. 26, 1491-1501.

Chaubey, A.K., Rizvi, I.A., 1999. Non-equilibrium effects in alpha induced reactions in some natural elements. Canadian Journal of Physics 67, 870-875.

Das, T., Pillai, M.R., 2013. Options to meet the future global demand of radionuclides for radionuclide therapy. Nucl. Med. Bio. 40, 23-32.

Delaunay-Olkowsky, J., Strohal, P., Cindro, N., 1963. Total reaction cross sections of proton induced reactions. Nucl. Phys. 47, 266-272.

Ditroi, F., Hermanne, A., Corniani, E., Takacs, S., Tárkányi, F., Csikai, J., Shubin, Y.N., 2009. Investigation of proton induced reactions on niobium at low and medium energies. Nucl. Inst. Meth. B 267, 3364-3374.

Ditrói, F., Takács, S., Tárkányi, F., Baba, M., Corniani, E., Shubin, Y.N., 2008. Study of proton induced reactions on niobium targets up to 70 MeV. Nucl. Inst. Meth. B 266, 5087-5100.

Dityuk, A.I., Lunev, V.P., Shubin, Y.N., Konobeyev, A.Y., 1998. New version of the advanced computer code ALICE-IPPE, Report INDC (CCP)-410, IAEA, Vienna.

EXFOR, http://www-nds.iaea.org/exfor/exfor.htm.

Fox, M.B., Voyles, A.S., Morrell, J.T., Bernstein, L.A., Lewis, A.M., Koning, A.J., Batchelder, J.C., Birnbaum, E.R., Cutler, C.S., Medvedev, D.G., 2021. Investigating high-energy proton-induced reactions on spherical nuclei: Implications for the preequilibrium exciton model. Phys. Rev. C 103, 034601.

Hussain, M., Ali, W., Amjed, N., Wajid, A.M., Aslam, M.N., 2022. An overview of nuclear data standardisation work for accelerator-based production of medical radionuclides in Pakistan. Radiochim. Acta 110, 645-662.

Kastleiner, S., Qaim, S.M., Nortier, F.M., Blessing, G., Van Der Walt, T.N., Coenen, H.H., 2002. Excitation functions of ^{85}Rb(p,xn)$^{85m, g, 83, 82, 81}$Sr reactions up to 100 MeV: integral tests of cross section data, comparison of production routes of ^{83}Sr and thick target yield of ^{82}Sr. Appl. Radiat. Isot. 56(5), 685-695.

Khandaker, M.U., Kim, K., Lee, M.W., Kim, K.S., Kim, G.N., Cho, Y.S., Lee, Y.O., 2009. Investigations of the ^{nat}Ti(p,x)^{43,44m,44g,46,47,48}Sc, ^{48}V nuclear processes up to 40 MeV. Appl. Radiat. Isot. 67, 1348-1354.

Kim, K., Kim, G., Shahid, M., Zaman, M., Yang, S.C., Uddin, M., Naik, H., 2018. Excitation functions of ^{93}Nb(p,x) reactions from threshold to 42.5 MeV. J. Radio. Anal. Nucl. Chem. 317, 1021-1031.

Koning, A.J., Delaroche, J.P., 2003. Local and global nucleon optical models from 1 keV to 200 MeV. Nucl. Phys. A 713, 231-310.

Koning, A.J., Rochman, D., 2012. Modern nuclear data evaluation with the TALYS code system. Nuclear Data Sheets 113(12), 2841-2934.

Lawriniang, B., Badwar, S., Ghosh, R., Jyrwa, B., Naik, H., Suryanarayana, S.V., Naik, Y.P., 2018. Excitation functions of proton-induced reactions on ^{nat}Fe and ^{nat}Zr targets for the production of cobalt and niobium isotopes. Eurs. Phys. J. A 54, 1-7.

Levkovskij, V.N., 1991. Activation cross section nuclides of average masses (A= 40-100) by protons and alpha-particles with average energies of (E= 10-50 MeV). Moscow, USSR.

Marik, J., Junutula, J., 2011. Emerging role of immunoPET in receptor targeted cancer therapy. Current Drug Delivery 8, 70-78.

Mercader, R.C., Caracoche, M.C., Mocoroa, A.B., 1972. Excitation functions for the production of ^{90}Nb and ^{88}Y by irradiation of zirconium with deuterons. Zeitschrift für Physik A Hadrons Nuclei 255, 103-111.

Morillon, B., Romain, P., 2007. Bound single-particle states and scattering of nucleons on spherical nuclei with a global optical model. Phys. Rev C 76, 044601–044611.

Mukherjee, S., Kumar, B.B., Rashid, M.H., Chintalapudi, S.N., 1997. α-particle induced reactions on yttrium and terbium. Phys. Rev. C 55, 2556-2562.

Murakami, M., Haba, H., Goto, S., Kanaya, J., Kudo, H., 2014. Production cross sections of niobium and tantalum isotopes in proton-induced reactions on ^{nat}Zr and natHf up to 14 MeV. Appl. Radiat. Isot. 90, 149-157.

Murata, T., Aikawa, M., Saito, M., Haba, H., Komori, Y., Ukon, N., Takács, S., Ditrói, F., 2019. Excitation function measurement for zirconium-89 and niobium-90 production using alpha-induced reactions on yttrium-89. Nucl. Instr. Meth. Phys. B 458, 21-27.

Nickles, R.J., 1991. A shotgun approach to the chart of the nuclides. Acta Radiol. Suppl. 376, 69-71.

NuDat 3.0, Data source :National Nuclear Data Center, Brookhaven National Laboratory,based on ENSDF and the Nuclear Wallet Cards, available from ⟨http://www.nndc.bnl.gov/nudat2⟩.

Otuka, N., Takacs, S., 2015. Definitions of radioisotope thick target yields. Radiochim. Acta 103, 1-6.

Perey, C.M., Perey, F.G., 1963. Deuteron optical model analysis in the range of 11 to 27 MeV. Phys. Rev. 132, 755-773.

Qaim, S.M., 1982. Nuclear data relevant to cyclotron produced short-lived medical radioisotopes. Radiochim. Acta, 147-162.

Qaim, S.M., 2004. Use of cyclotrons in medicine. Radiat. Phys. Chem. 71, 917-926.

Qaim, S.M., 2011. Development of novel positron emitters for medical applications: nuclear and radiochemical aspects. Radiochim. Acta 99, 611-625.

Qaim, S.M., 2012. The present and future of medical radionuclide production. Radiochim. Acta 100, 635-651.

Qaim, S.M., 2017. Nuclear data for production and medical application of radionuclides: Present status and future needs. Nuc. Med. Bio. 44, 31-49.

Qaim, S.M., 2003. Cyclotron production of medical radionuclides. Kluwer,, Dordrecht, The Netherlands,.

Qaim, S.M., Spahn, I., 2018. Development of novel radionuclides for medical applications. J. Label. Compd. Radiopharm. 61(3), 126-140.

Qaim, S.M., Steyn, G.F., Spahn, I., Spellerberg, S., Van Der Walt, T.N. and Coenen, H.H., 2007. Yield and purity of ^{82}Sr produced via the ^{nat}Rb(p, xn)^{82}Sr process. Appl. Radiat. Isot.65, 247-252.

Qaim, S.M., Sudár, S., Scholten, B., Koning, A.J., Coenen, H.H., 2014. Evaluation of excitation functions of ^{100}Mo(p,d+pn)^{99}Mo and ^{100}Mo(p,2n)^{99m}Tc reactions: Estimation of long-lived Tc-impurity and its implication on the specific activity of cyclotron-produced ^{99m}Tc. Appl. Radiat. Isot. 85.

Radchenko, V., Bouziotis, P., Tsotakos, T., Paravatou-Petsotas, M., de la Fuente, A., Loudos, G., Harris, A.L., Xanthopoulos, S., Filosofov, D., Hauser, H., 2016. Labeling and preliminary

in vivo assessment of niobium-labeled radioactive species: A proof-of-concept study. Nucl. Med. Bio. 43, 280-287.

Radchenko, V., Filosofov, D.V., Bochko, O.K., Lebedev, N.A., Rakhimov, A.V., Hauser, H., Eisenhut, M., Aksenov, N.V., Bozhikov, G.A., Ponsard, B., 2014. Separation of ^{90}Nb from zirconium target for application in immuno-PET. Radiochim. Acta 102, 433-442.

RIPL-3, d., International Atomic Energy Agency, Vienna. Available from www.ds-iaea.org/RIPL-3/.

Shahid, M., Kim, K., Naik, H., Zaman, M., Kim, G., Yang, S.C., Song, T.Y., 2015. Measurement of excitation functions in alpha-induced reactions on yttrium. Nucl. Inst. Meth. B 342, 158-165.

Singh, N.L., Gadkari, M.S., Chintalapudi, S.N., 2000. Measurement and analysis of alpha particle induced reactions on yttrium. Physica Scripta 61, 550.

Skakun, E.A., Batij, V.G., Rakivnenko, Y.N., Rastrepin, O.A., 1987. Excitation functions and isomer ratio for up-to-9 MeV proton interactions with Zr and Mo isotope nuclei. Yadernaya Fizika 46, 28-39.

Sudár, S., Cserpák, F., Qaim, S.M., 2002. Measurements and nuclear model calculations on proton induced reactions on ^{103}Rh upto 40 MeV: Evaluation of the excitation function of the ^{103}Rh(p,n)^{103}Pd reaction relevant to the production of the therapeutic radionuclide ^{103}Pd. Appl. Radiat. Isot. 56, 821-831.

Szelecsényi, F., Steyn, G.F., Kovács, Z., Vermeulen, C., Nagatsu, K., Zhang, M.R., Suzuki, K., 2015. Excitation functions of ^{nat}Zr+p nuclear processes up to 70 MeV: new measurements and compilation. Nucl. Inst. Meth. B 343, 173-191.

Tárkányi, F., Ditroi, F., Takacs, S., Hermanne, A., Al-Abyad, M., Yamazaki, H., Baba, M., Mohammadi, M.A., 2015. New activation cross section data on longer lived radionuclei produced in proton induced nuclear reaction on zirconium. Appl. Radiat. Isot. 97, 149-169.

Tárkányi, F., Ignatyuk, A.V., Hermanne, A., Capote, R., Carlson, B.V., Engle, J.W., Verpelli, M., Kellett, M.A., Kibedi, T., Kim, G., N., Kondev, F.G., Hussain, M., 2019. Recommended nuclear data for medical radioisotope production: diagnostic positron emitters. J. Radioanal. Nucl. Chem. 319, 533-666.

Tárkányi, F., Takács, S., Gul, K., Hermanne, A., Mustafa, M.G., Nortier, M., Oblozinsky, P., Qaim, S.M., Scholten, B., Shubin, Y.N., Youxiang, Z., 2001. Charged particle cross-section data base for medical radioisotope production: diagnostic radioisotopes and monitor reactions. . IAEA-TECDOC-1211, 49-97.

Titarenko, Y.E., Batyaev, V.F., Titarenko, A.Y., Butko, M.A., Pavlov, K.V., Florya, S.N., Tikhonov, R.S., Zhivun, V.M., Ignatyuk, A.V., Mashnik, S.G., 2011. Measurement and simulation of the cross sections for nuclide production in natW and ^{181}Ta targets irradiated with 0.04-to 2.6-GeV protons. Physics of Atomic Nuclei 74, 551-572.

Uddin, M.S., Khandaker, M.U., Kim, K.S., Lee, Y.S., Lee, M.W., Kim, G.N., 2008. Excitation functions of the proton induced nuclear reactions on natural zirconium. Nucl. Inst. Meth. B 266, 13-20.

Uddin, M.S., Sudár, S., Hossain, S.M., Khan, R., Zulquarnain, M.A., Qaim, S.M., 2013. Fast neutron spectrum unfolding of a TRIGA Mark II reactor and measurement of spectrum-

averaged cross sections: integral tests of differential cross sections of neutron threshold reactions. Radiochim. Acta 101, 613-620.

Usher, O.H., Arizmendi, C.M., Wasilevsky, C., Nassiff, S.J., 1976. Production cross sections and isomeric ratios for the isomeric pair ^{89m}Nb and ^{89g}Nb in the ^{90}Zr(d,3n)$^{89m/g}$Nb reaction. Radiochim. Acta 23, 159-160.

van Dongen, G.A., Vosjan, M.J., 2010. Immuno-positron emission tomography: shedding light on clinical antibody therapy. Cancer Biothe. Radiopharma. 25, 375-385.

Voyles, A.S., Bernstein, L.A., Birnbaum, E.R., Engle, J.W., Graves, S.A., Kawano, T., Lewis, A.M., Nortier, F.M., 2018. Excitation functions for (p,x) reactions of niobium in the energy range of Ep= 40–90 MeV. Nucl. Inst. Meth. B 429, 53-74.

Wu, A.M., 2009. Antibodies and antimatter: the resurgence of immuno-PET. J. Nucl. Med. 50, 2-5.

Yang, S.C., Jung, M.H., Kim, G., Lee, Y.O., 2018. Measurement of production cross sections in proton induced reactions on natural zirconium. Nucl. Inst. Meth. B 436, 179-185.

List of Figure Captions

Figure 1 Normalized experimental data and results of nuclear model calculations for the ^{90}Zr(p,n)^{90}Nb reaction

Figure 2 Ratio of measured cross section to model calculation by TALYS, plotted as a function of proton energy.

Figure 3 Selected experimental data and recommended Cross section curve with 95% upper and lower confidence limits for the ^{90}Zr(p,n)^{90}Nb and ^{90}Zr(p,2n)^{89}Nb reactions. Due to insufficient available experimental information, the latter curve should be regarded as reference curve.

Figure 4 Normalized experimental data and results of nuclear model calculations for the ^{91}Zr(p,2n)^{90}Nb reaction.

Figure 5 Selected experimental data and recommended cross section curve with 95% upper and lower confidence limits for the ^{91}Zr(p,2n)^{90}Nb reaction. The curves for ^{91m}Nb and ^{89}Nb are based on purely calculated cross sections.

Figure 6 Normalized experimental data and results of nuclear model calculations for the ^{90}Zr(d,2n)^{90}Nb reaction.

Figure 7 Selected experimental data and suggested cross section curve with 95% upper and lower confidence limits for ^{90}Zr(d,2n)^{90}Nb and ^{90}Zr(d,3n)^{89}Nb reactions.

Figure 8 Normalized experimental data and results of nuclear model calculations for the ^{89}Y(α,3n)^{90}Nb reaction.

Figure 9 Selected experimental data and recommended Cross section curve with 95% upper and lower confidence limits for the ^{89}Y(α,3n)^{90}Nb and ^{89}Y(α,4n)^{89}Nb reactions. Encircled data points are discarded.

Figure 10 Normalized experimental data and recommended cross section curve with 95% upper and lower confidence limits for the ^{89}Y(α,n)^{92m}Nb and ^{89}Y(α,2n)^{91m}Nb reactions. Encircled data points are discarded.

Figure 11 Normalized experimental data and theoretical curves for the ^{93}Nb(p,4n)^{90}Mo reaction.

Figure 12 Normalized experimental data and recommended cross section curve with 95% upper and lower confidence limits for the ^{93}Nb(p,4n) ^{90}Mo reaction.

Fig 13. Experimental data and evaluated Curve for ^{nat}Zr(p,x)^{90}Nb reaction. The solid curve is based on a normalization of the evaluated data of the ^{90}Zr(p,n)^{90}Nb and ^{91}Zr(p,2n)^{90}Nb reactions to ^{nat}Zr as target.

Figure 14 Integral yields of the ^{90}Zr(p,n)^{90}Nb and ^{90}Zr(p,2n)^{89}Nb reactions calculated from our evaluated curves, and comparison with the experimentally determined thick target yields of ^{90}Nb by Busse et al. (2002).

Figure 15 Calculated integral yields of the ^{91}Zr(p,2n)^{90}Nb and ^{91}Zr(p,3n)^{89}Nb reactions

Figure 16 Calculated integral yields of the ^{90}Zr(d,2n)^{90}Nb and ^{90}Zr(d,3n)^{89}Nb reactions.

Figure 17 Calculated integral yields of the ^{89}Y(α,3n)^{90}Nb and ^{89}Y(α,4n)^{89}Nb reactions.

Figure 18 Comparison of production routes of ^{90}Nb on the basis of their integral yields as well integral yield of the precursor ^{90}Mo.

List of Table Captions

Table 1: Decay Characteristics of ^{90}Nb and relevant accompanying radionuclides

Radionuclide	**Half-life** $T_{1/2}$	**Decay mode (%)**	**γ-ray energy (keV)**	**Abundance of γ-ray (%)**
^{90}Nb	14.6 h	EC (47) β^+ (53)	132.72 141.18 1129.22	4.13 66.8 92.7
^{89}Nb	2.03 h	EC (100)	1127 1833.4	2.1 3.3
^{91m}Nb	60.86 d	EC (3.4) IT (96.6)	1204.67 104.62	2.0 0.574
^{92m}Nb	10.15 d	EC (100)	934.44	99.15
^{90}Mo	5.56 h	EC (100)	122.37 257.34	64 77

* taken from NuDat 3.0 (2022) (NuDat 3.0) except for EC and β^+ branching values which were taken from Browne and Firestone (1986), Table of radioactive isotopes. Wiley, New York

Table:2 Investigated nuclear reactions for the production of ^{90}Nb, ^{89}Nb, and ^{91m}Nb with their Q values, threshold energies, and references

Nuclear reaction	Q-Value (MeV)	Threshold energy (MeV)	References
^{90}Zr(p,n)^{90}Nb	-6.8	6.9	(Busse et al., 2002; Delaunay-Olkowsky et al., 1963; Levkovskij, 1991; Skakun et al., 1987)
^{90}Zr(p,2n)^{89}Nb	-17.0	17.1	(Biryukov et al., 1980; Busse et al., 2002)
^{91}Zr(p,n)^{91m}Nb	-2.0	2.1	(Biryukov et al., 1980; Blaser et al., 1951)
^{91}Zr(p,2n)^{90}Nb	-14.1	14.2	(Levkovskij, 1991)
^{90}Zr(d,2n)^{90}Nb	-16.3	16.6	(Mercader et al., 1972)
^{90}Zr(d,3n)^{89}Nb	-26.4	27.0	(Usher et al., 1976)
^{89}Y(α,2n)^{91m}Nb	-14.7	15.8	(Murata et al., 2019; Shahid et al., 2015)
^{89}Y(α,3n)^{90}Nb	-26.8	28.04	(Chaubey and Rizvi, 1999; Levkovskij, 1991; Mukherjee et al., 1997; Murata et al., 2019; Shahid et al., 2015; Singh et al., 2000)
^{89}Y(α,4n)^{89}Nb	-36.9	38.6	(Chaubey and Rizvi, 1999; Murata et al., 2019)
^{93}Nb(p,4n)^{90}Mo→^{90}Nb	-32.037	32.384	(Ditroi et al., 2009; Ditrói et al., 2008; Fox et al., 2021; Kim et al., 2018; Titarenko et al., 2011; Voyles et al., 2018)

Table 3 Reference cross sections for the formation of ^{90}Nb and ^{89}Nb in proton-induced reactions on ^{90}Zr

Energy (MeV)	^{90}Zr(p,n)^{90}Nb			^{90}Zr(p,2n)^{89}Nb		
	Cross section (mb)	95% confidence limits		Cross section (mb)	95% confidence limits	
		lower	upper		lower	upper
8	154	204	104			
9	388	444	332			
10	569	635	502			
11	668	729	607			
12	722	779	666			
13	742	802	683			
14	741	803	680			
15	712	770	655			
16	628	676	580			
17	510	551	468			
18	386	423	350	133	146	120
19	285	315	255	265	277	252
20	206	230	183	365	376	353
21	161	180	141	434	445	424
22	127	143	111	476	486	467
23	107	121	94	494	504	485
24	91	102	80	492	502	482
25	80	89	71	473	483	464
26	71	79	62	442	451	433
27	64	73	55	402	411	394
28	58	66	49	358	366	349
29	57	66	49	311	320	302
30				264	273	255

34				120	128	111
36				82	91	73
38				64	73	55
40				60	69	51

Table 4 Reference cross sections for the formation of ^{91m}Nb, ^{90}Nb and **^{89}Nb in proton-induced reactions on ^{91}Zr**

Energy (MeV)	^{91}Zr(p,2n)^{90}Nb			^{91}Zr(p,3n)^{89}Nb			^{91}Zr(p,n)^{91m}Nb		
	Cross section (mb)	95% confidence limits lower	upper	Cross section (mb)	95% confidence limits lower	upper	Cross section (mb)	95% confidence limits lower	upper
5							72	38	105
6							213	181	245
7							375	346	403
8							523	497	550
9							639	613	665
10							712	685	738
11							740	714	766
12							727	701	752
13							679	655	703
14							607	584	630
15	150	173	127				519	496	542
16	345	385	304				425	401	448
17	498	558	437				332	308	356
18	585	650	520				247	223	271
19	643	717	568				175	151	198
20	704	784	624				118	95	141
21	711	784	638				77	55	100
22	728	803	653				52	30	75
23	715	790	641				41	18	64
24	701	770	632				40	16	63
25	649	716	583	0	0	0	45	21	69
26	583	649	517	17	17	17	54	30	78
27	494	550	437	62	62	62	62	39	86
28	397	452	342	113	113	113	68	45	92
29	332	380	284	162	162	162	64	40	88
30	320	417	224	204	204	204			
31				236	236	236			
32				256	256	256			
33				267	267	267			
34				268	268	268			
35				261	261	261			
36				250	250	250			
37				234	234	234			
38				217	217	217			
39				199	199	199			

40				180	180	180			

Table 5 Reference cross sections for the formation of ^{90}Nb and ^{89}Nb in deuteron-induced reactions on ^{90}Zr

Energy (MeV)	^{90}Zr(d,2n)^{90}Nb			^{90}Zr(d,3n)^{89}Nb		
	Cross section (mb)	95% confidence limits lower	upper	Cross section (mb)	95% confidence limits lower	upper
6						
7						
8						
9						
10	60	40	80			
11	197	177	216			
12	352	333	371			
13	506	489	523			
14	646	630	662			
15	762	747	777	0	0	0
16	849	833	864	5	4	7
17	904	889	920	21	19	23
18	930	914	945	45	40	49
19	927	912	942	74	67	80
20	900	886	914	106	97	114
21	853	839	867	139	129	149
22	792	778	806	171	160	183
23	722	707	736	201	188	214
24	647	632	661	227	213	241
25	572	558	587	248	232	263
26	501	487	516	263	246	279
27	437	423	451	272	254	289
28	381	367	395	274	256	292
29	334	320	348	271	253	289
30	297	282	312	263	245	280
31	268	253	284	250	234	267
32	246	231	262	234	218	249
33	230	214	245	215	201	229
34	216	201	231	195	182	209
35	203	188	219	176	163	189
36	191	173	208	142	129	155
37	178	159	197	121	110	132
38	166	146	185	114	103	125
39	158	138	178	113	101	124
40	162	128	195	93	74	111

Table 6 Recommended cross sections for the formation of ^{90}Nb and **^{89}Nb in alpha-particle induced reactions on ^{89}Y**

Energy	^{89}Y(α,3n)^{90}Nb	^{89}Y(α,4n)^{89}Nb

(MeV)	Cross section (mb)	95% confidence limits		Cross section (mb)	95% confidence limits	
		lower	upper		lower	upper
29	27	39	22			
30	98	117	84			
31	215	245	186			
32	349	398	303			
33	487	556	421			
34	616	703	526			
35	719	813	611			
36	791	878	675			
37	847	925	726			
38	890	971	758			
39	911	1011	771			
40	917	1028	776			
41	905	1008	769	10	10	11
42	880	970	746	29	28	30
43	846	927	710	52	51	53
44	831	910	688	77	76	79
45	816	897	670	104	102	106
46	753	836	607	131	128	133
47	680	776	520	157	154	160
48	594	705	419	182	179	185
49	518	630	341	205	202	209
50	422	515	239	226	222	230
52				260	256	264
54				282	277	286
56				291	286	296
58				288	283	294
60				276	271	281

62				256	252	261
64				231	227	236
66				204	199	209
68				177	173	181
70				164	160	168

Table 7 Recommended cross sections for the formation of ^{90}Mo in proton-induced reactions on ^{93}Nb

Energy (MeV)	^{93}Nb(p,4n)^{90}Mo→^{90}Nb					
	Cross section (mb)	95% confidence limits		Cross section (mb)	95% confidence limits	
		lower	upper		lower	upper
35	0	0	1	63	33	21
36	1	0	1	64	31	19
37	1	0	2	65	29	18
38	2	1	4	66	28	17
39	3	1	5	67	26	16
40	5	2	8	68	25	15
41	8	3	13	69	23	14
42	12	5	19	70	21	12
43	19	8	29	71	20	10
44	29	15	43	72	18	6
45	40	22	57	73	16	3
46	50	30	70	74	14	1
47	63	40	87	75	13	3
48	72	47	96	76	13	5
49	74	52	96	77	13	3
50	79	58	101			
51	81	60	101			
52	80	60	100			
53	77	58	95			
54	70	52	87			
55	64	47	81			
56	60	43	76			
57	55	39	72			
58	49	34	63			

59	44	31	58			
60	40	27	53			
61	38	25	50			
62	35	23	47			

Table 8: Optimized energy ranges along with the thick target yield values of the products

Nuclear reaction	**Energy range (MeV)**	**Thick target yield of ^{90}Nb (MBq/μAh)**	**Radionuclidic impurity (%)**		
			^{89}Nb	**^{91m}Nb**	**^{92m}Nb**
^{90}Zr(p,n)^{90}Nb	**16→8**	**482**	0	-	-
^{91}Zr(p,2n)^{90}Nb	**24→15**	**747***	0	0.17	-
^{90}Zr(d,2n)^{90}Nb	**21→12**	**519***	1	-	-
^{89}Y(α,3n)^{90}Nb	**39→31**	**53**	0.04	0.03	0.003
^{93}Nb(p,4n) ^{90}Mo→^{90}Nb	**80→40**	**440**	0	0	0

* Yield was calculated using reference values